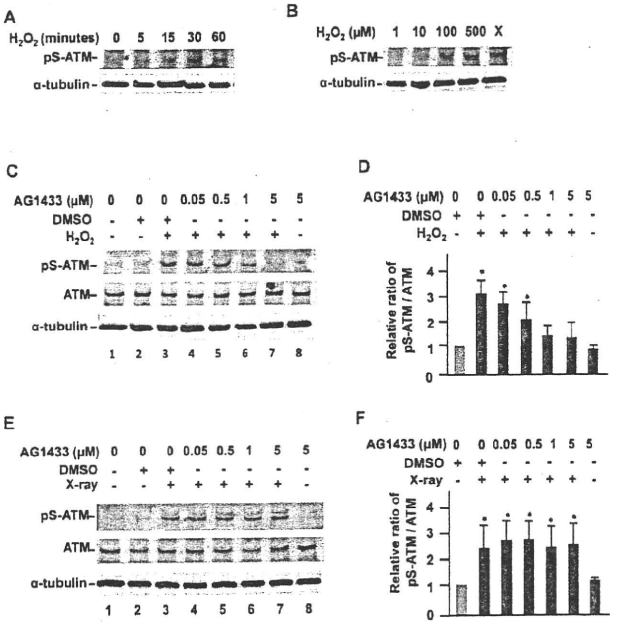

Fig. 3. AG1433 suppressed the activation of ATM in response to oxidative stress. P19 cells were used at day 5 during neuronal differentiation. (A) ATM activation in response to oxidative stress with hydrogen peroxide (100 μM) for the indicated time points (0, 5, 15, 30 and 60 minutes). (B) ATM activation at different concentrations of hydrogen peroxide dose (1, 10, 100, 500 μM); cells were harvested 30 minutes after treatment. 'X' indicates stimulation with 10 Gy X-ray irradiation for comparison. (C) Cells were treated with hydrogen peroxide (100 μM) for 30 minutes to activate ATM (lane 3-7). The activation of ATM was suppressed by adding AG1433, an inhibitor of PDGFRB and VEGFR-2; AG1433 was dissolved in DMSO and added at different concentrations (lane 4-7). A control experiment was performed with 0.1% DMSO using the same concentration of solvent as for AG1433 (5 μM) (lane 3). (D) The experiments were repeated and measured in triplicate. The ratios of pS-ATM to ATM were analyzed statistically. (E) After treatment of cells with 10 Gy X-rays, and harvesting 1 hour later, ATM was activated (lane 3-7), and activation was not suppressed by adding AG1433. A control experiment was performed with 0.1% DMSO (lane 3). (F) The experiments were repeated and measured in triplicate. The ratios of pS-ATM to ATM were analyzed statistically. The results of western blotting were quantified and subjected to statistical analysis using the Mann-Whitney U-test with Bonferroni Correction. *P<0.05. Error bars represent s.e.m. from three independent experiments.

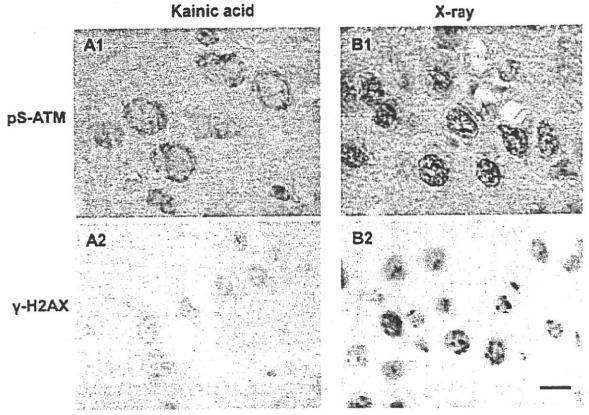

Fig. 4. Differential subcellular localization of activated ATM in neurons. Adult mice were treated with kainic acid (A1, A2; 30 mg/kg, i.p.) or X-ray irradiation (B1, B2; 10 Gy) and activation of ATM (pS-ATM) in neurons of the cerebral cortex was investigated. We observed pS-ATM in the cytoplasm after treatment with kainic acid for 4 hours (A1) and in the nucleus 4 hours after irradiation by 10 Gy X-ray (B1). γ-H2AX was observed in the nucleus after exposure to X-ray irradiation (B2), but not detected in the neurons treated with kainic acid. Scale bar: 10 μm.

(supplementary material Fig. S4). Recently, activation of ATM has been demonstrated in the cytoplasm in response to oxidative stress, which was shown to be independent of its activation in the nucleus by the same agent (Alexander et al., 2010). We failed initially to distinguish the distinct activation of ATM in cytoplasm from that in the nucleus because of the degree of oxidative stress induced (supplementary material Fig. S4). Therefore, we designed more-physiological oxidative stress conditions for neurons to investigate activation of ATM in the cytoplasm independent of that in the nucleus.

Although multiple factors can precipitate oxidative stress in neurons, the neurotransmitter glutamic acid is a major factor that induces excitotoxicity of neurons in the brain. Kainic acid (KA) is a potent glutamate receptor agonist with selectivity towards non-NMDA-type glutamate receptors (Olney et al., 1974). We applied a KA stimulation model to induce metabolic oxidative stress in mouse neurons (Coyle and Puttfarcken, 1993; Zhang et al., 2002). KA stimulation caused two types of seizures in these animals. One case showed repeated bending movement of the head. Another case showed abnormal continuous muscle contraction (supplementary material Movie 1), and induced distinct activation of ATM in the mouse brain at the cerebral cortex, hippocampus and deep cerebellar nuclei (DCN) (supplementary material Fig. S5). We found activated ATM predominantly in the cytoplasm (Fig. 4A1; supplementary material Fig. S6) in the absence of γ-H2AX induction (Fig. 4A2; supplementary material Fig. S6). By contrast, X-ray irradiation induced genotoxic stress and ATM was activated in the nucleus (Fig. 4B1; supplementary material Fig. S6) associated with γ-H2AX foci (Fig. 4B2; supplementary material Fig. S6). We observed distinct vacuolar formation in neurons in DCN by stimulation with KA (supplementary material Fig. S5B3).

Suppression of PDGFRB in DCN of ATM-deficient mice

We examined in more detail the relationship between ZFHX3 and PDGFRB expression in P19 cells before and after neuronal differentiation. A prominent increase of ZFHX3 and PDGFRB protein expression was observed in the terminally differentiated P19 neuron-like cells at day 7 (Fig. 5A). Screening analysis by in situ hybridization (http://developingmouse.brain-map.org/data/Pdgfrb.html) showed that PDGFRB was highly expressed in DCN. Immunohistochemistry revealed distinct staining of ZFHX3 (Fig. 5C4,C5) and PDGFRB (Fig. 5C6,C7) in large neurons of the DCN of adult control mouse brain, but expression of both proteins was strongly suppressed in ATM-deficient mice (Fig. 5C11-C14). BrdU staining was used in an embryonic rat to distinguish proliferating (Fig. 5B2i) and post-mitotic (Fig. 5B2ii) cells. The correlated

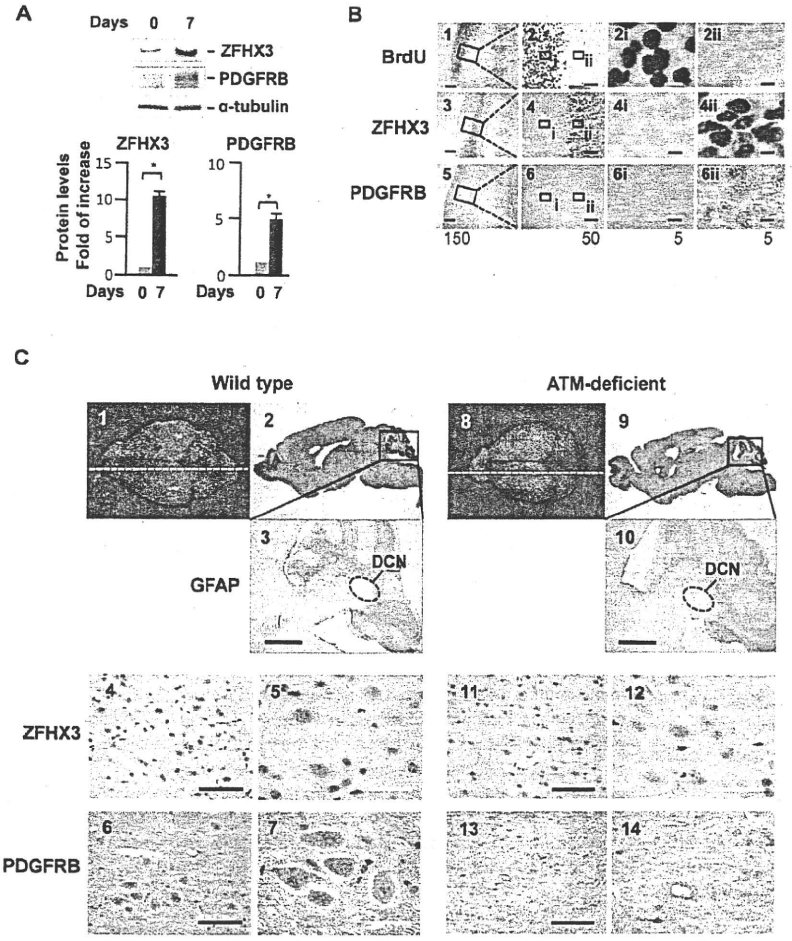

Fig. 5. PDGFRB is expressed in neurons specifically in deep cerebellar nuclei. (A) Western blot analysis showed that the expression of PDGFRB correlated with ZFHX3 and was at the highest level at day 7 of neuronal differentiation of P19 cells. Statistical analysis used the Mann-Whitney *U*-test: **P*<0.01. Error bars represent s.e.m. from three independent experiments. (B) Rat embryo (E14) spinal cord exhibited a proliferating field stained by BrdU (2i), and a post-mitotic field negative for BrdU showed staining for ZFHX3 (4ii) and PDGFRB (6ii). Scale bars are indicated at the bottom of the panels. (C) Immunohistochemical analysis of para-sagittal sections of wild-type mouse and ATM-deficient mouse brain, indicated by white dotted lines, stained with hematoxylin and eosin (HE) (2 and 8); magnification of cerebellum stained with glial fibrillary acidic protein (GFAP) counterstained with hematoxylin (3 and 10) – dotted-line circles designate the region of DCN; ZFHX3 expression (4 and 5; 11 and 12); PDGFRB expression (6 and 7; 13 and 14). Scale bars in panels 3 and 10: 500 μm. Scale bars (black) in panels 4, 6, 11, 13: 50 μm. Scale bars (white) in panels 5, 7, 12, 14: 20 μm.

expression of ZFHX3 and PDGFRB in the post-mitotic neurons was consistent with the results of the microarray analysis using a model of neuronal differentiation (supplementary material Table S1). Suppression of PDGFRB in DCN of the ATM-deficient mouse might account for the mechanisms of specific neurodegeneration in the cerebellum.

DISCUSSION

The data described here provide further support for a role for cytoplasmic ATM activation in protection against neuronal cell death. It is well established that a significant amount of ATM protein is present in the cytoplasm of a variety of cell types including neurons (Kuljis et al., 1999; Barlow et al., 1996; Boehrs et al., 2007) (Gorodetsky et al., 2007). More recently Li et al. (Li et al., 2009) showed that cytoplasmic ATM modulates synaptic function. They demonstrated that ATM forms a complex with the synaptic vesicle proteins VAMP2 and synapsin-1 and is responsible for phosphorylation of these proteins. These data suggest that a non-nuclear role for ATM might be important in protecting against neurodegeneration. Alexander et al. (Alexander et al., 2010) have shown that reactive oxygen species rapidly activate ATM in the cytoplasm to repress the kinase mTOR in the mammalian target of rapamycin complex 1 (mTORC1) and induce autophagy. This does not involve signaling from DNA DSBs and the authors make the intriguing suggestion that this activation might involve the oxidation of sulfhydryl groups on ATM to alter its conformation.

In this study, we show that ATM induces *ZFHX3* expression during RA-induced neuronal differentiation of P19 cells by activation and binding of CREB to a CRE consensus site located in the *ZFHX3* promoter. We also show that ZFHX3 regulates target genes that encode cell adhesion molecules (procollagen type III α1, integrin α8) as well as PDGFRB. PDGFRB is a key regulator not only for connective tissue cells in the induction of adhesion molecules but also for neurons in protection from glutamatergic excitotoxicity (Ishii et al., 2006). Notably, we showed that PDGFRB and/or VEGFR-2 positively supported ATM activation in response to oxidative stress in neurons. We identified significant elevation of *Pdgfrb* and *Vegfr-2* mRNA in P19-derived neuron-like cells (supplementary material Fig. S7). Although neurons are highly susceptible to oxidative stress because of their high rate of oxidative metabolism and low level of antioxidant enzymes (Brooks et al., 2000), membrane receptors might immediately respond to oxidative stress through the activation of ATM in the cytoplasm to protect neurons.

We revealed here the activation of ATM in the cytoplasm in response to excessive excitation of neurons. The excitation of

neurons induces metabolic oxidative stress that is a causal, or at least an ancillary, factor of chronic neurodegenerative disorders (Coyle and Puttfarcken, 1993). We showed that PDGFRB and/or VEGFR-2 were required for the activation of ATM in response to oxidative stress. The suppression of PDGFRB in DCN of ATM-deficient mice provides an explanation for the reduction of response to oxidative stress. We observed a high incidence of vacuolar formation specifically in DCN (supplementary material Fig. S5B3), where PDGFRB was highly expressed (Fig. 5C6,C7). Neurons in the DCN are directly innovated by Purkinje cells and most output fibers of the cerebellum originate from these nuclei (supplementary material Fig. S8). Damage of DCN would inevitably induce degeneration of Purkinje cells by loss of direct synaptic connections. We consider the functional unit of Purkinje cells and DCN as important to the etiology of A-T. The distinct activation of ATM in the cytoplasm at the DCN caused by KA stimulation indicated the protective response to oxidative stress induced by the excessive neuronal excitation in these neurons. In particular, DCN responded most strongly to show vacuolar formation. This phenomenon might be related to the fact that the activation of ATM in the cytoplasm induces autophagy via suppression of mTOR (Alexander et al., 2010). We observed intensive accumulation of microtuble-asssociated protein light chain 3 (LC3) in DCN in response to KA treatment (supplementary material Fig. S9). Although the autophagic response was believed to promote acute neuron death because of destruction of organelles through this process (Wang et al., 2008), the study of chronic neurodegenerative disease revealed that autophagy was not the primary cause of neuron death but rather was a protective mechanism for the function of neurons by clearing dysfunctioning organelles. Impaired autophagy is implicated in Parkinson's disease in the accumulation of dysfunctional mitochondria, leading to neurons loss (Narendra et al., 2008). We should further study the mechanism of the autophagy in response to oxidative stress in relation to the activation of ATM in these neurons.

Expression microarray analysis revealed that ZFHX3 significantly activated most types of procollagen genes except type II, an essential component of the extracellular matrix during wound healing. Because collagen type II is a specific component of cartilage (Cheah et al., 1985), it is reasonable that this type of collagen is not expressed in a model of neuronal differentiation. PDGFRB protein becomes prominent in vessels in the proliferating tissue zone in wounds as early as the first day after surgery (Reuterdahl et al., 1993). Because ZFHX3 regulates procollagen genes as well as PDGFRB, it would be expected to play a crucial role during wound healing. Therefore, malfunction of ZFHX3 might be expected to induce circulatory diseases. Recently, variants in *ZFHX3* have been identified that are associated with genetic susceptibility to Kawasaki disease, with increasing risk of aneurismal dilatation in the heart (Burgner et al., 2009). Variants in *ZFHX3* are also associated with susceptibility to atrial fibrillation and ischemic stroke (Benjamin et al., 2009; Gudbjartsson et al., 2009). These linkage studies suggest an important role of ZFHX3 in the wound healing process in damaged blood vessels. Notably, PDGFRB is highly expressed in the cerebellum (Lein et al., 2007), the area of the brain that undergoes the specific neurodegeneration that characterizes A-T.

In summary, we propose here three different pathways to trigger the activation of ATM (Fig. 6). The first, signaling from DNA DSBs, induces the activation of ATM at foci in the nucleus. The second, retinoic acid stimulation (Fernandes et al., 2007), activates ATM in a diffuse pattern in the nucleus (Bakkenist and Kastan, 2003). The third, oxidative stress, induces activation of ATM in the cytoplasm (Alexander et al., 2010), which is the pathway in response to neuronal excitation. We found membrane-bound tyrosine kinases are required to trigger the activation of ATM under oxidative stress, which is independent from the response to genotoxic stress. Once activated, ATM can induce autophagy by suppressing mTOR to enhance clearance of damaged organelles. Overall, the observations support a role for cytoplasmic ATM in protecting neurons against oxidative stress and chronic neuronal degeneration.

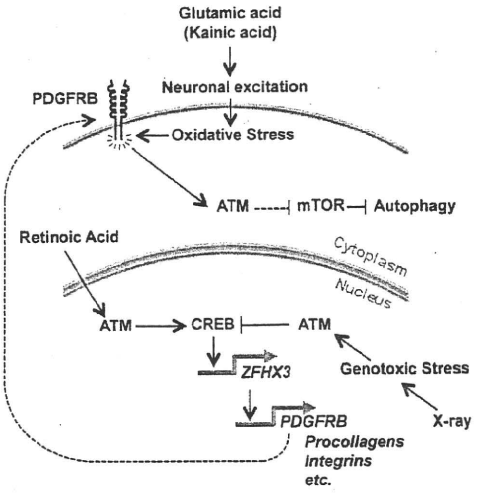

Fig. 6. A signaling pathway from ATM to ZFHX3 for the expression of PDGFRB that is required for the activation of ATM in response to oxidative stress in the cytoplasm. Activation of ATM kinase by retinoic acid stimulation relays to phosphorylation of CREB at Ser133 for the activation of target genes. By contrast, X-ray irradiation induces activation of ATM at the foci of DNA DSBs. The genotoxic stress induces extra phosphorylation of CREB at Thr100, Ser111, Ser121 to decrease transactivation potential (Shi et al., 2004). In the retinoic-acid-stimulated signal pathway, CREB induces ZFHX3 expression by binding to CRE (5′-TGACGTCA-3′) in the *ZFHX3* (neuron-specific) promoter located 5.5 kb upstream from the initiation site of *ZFHX3* transcription. ZFHX3 activates genes for cell adhesion molecules (procollagens, integrins) and PDGFRB for the survival of neurons. The activation of ATM in the cytoplasm in response to oxidative stress relays signals from PDGFRB to LKB1, AMPK, TSC2 and mTOR to maintain homeostasis of organelles by activating autophagy (Alexander et al., 2010).

METHODS

Cell culture

P19 mouse embryonal carcinoma cells were maintained in α-MEM (Rudnicki and McBurney, 1987). To induce neuronal differentiation, P19 cells were grown as aggregates on bacterial-grade dishes for 4 days with 0.5 μM all-trans retinoic acid (RA) (Sigma, USA) and 10% fetal bovine serum (FBS). Cells were cultured in α-MEM containing 1% FBS without RA on glass slides coated with combinations of 0.01% poly-L-lysine (P8920, Sigma) for 3 hours and 1 μg/ml bovine plasma fibronectin (Invitrogen, USA) overnight

at room temperature. Where indicated, the ATM kinase inhibitor KU-55933 [2-morpholin-4-yl-6-thianthren-1-yl-pyran-4-one; 2-morpholino-6-(thianthren-1-yl)-4H-pyran-4-one (Calbiochem, USA)] (10 μM) was added to the culture medium every day, and AG1433 [2-(3,4-dihydroxyphenyl)-6,7-dimethylquinoxaline (Calbiochem, USA)], a specific inhibitor of PDGFRB and VEGFR-2, at the series of concentrations of 0.05, 0.5, 1.0, 5.0 μM was added 30 minutes before adding hydrogen peroxide.

Mice

ATM-wild-type and ATM-deficient mice (provided by P. Leder, Harvard Medical School, Boston, MA) were maintained under ambient conditions (23°C, 55% humidity) with controlled light and dark cycles. Genomic DNA was isolated from tail tips and used to amplify a PCR product of the mouse *Atm* gene by using the following primers: KO-1F, 5′-TGGTCAGTGTAACAGTCATTGTGC-3′; KO-1R, 5′-AAGGTTGTAGATAGGTCAGCATTG-3′; KO-2R, 5′-AACGAGATCAGCAGCCTCTGTTCC-3′. Primer KO-1F is located 220 bp upstream (intron 34) of exon 34, primer KO-1R is located 123 bp into exon 34, and primer KO- 2R is located 87 bp into the poly(A) region of *PGKneo*. These primers generate a PCR product of 342 bp from wild-type animals and a targeted PCR product of 406 bp from $Atm^{-/-}$ mice. Kainic acid [2-carboxy-3-carboxymethyl-4-isopropenyl-pyrrolidine (Enzo Life Science, USA)] was administered [30 mg/kg, intraperitoneal (i.p.)] to male DDY mice. The whole brain was isolated from 3-month-old mice after perfusion fixation with 4% paraformaldehyde. Pregnant rats (Std Wister ST) were administered 5-bromo-2′-deoxy-uridine (BrdU, 50 mg/kg) for 3 hours to label E14.5 embryos. The embryos were then dissected out, and their brains were fixed in 4% paraformaldehyde and embedded in paraffin.

X-ray irradiation

Cells or mice were X-ray-irradiated at a dose rate of 10 Gy using X-ray machine CAX-210 (Chubu Medical Co. Ltd, Yokkaichi, Japan) operating at 210 kV, 10 mA, for 4 minutes 45 seconds with copper shield.

Transfection and plasmid constructs

To generate a series of luciferase reporter plasmids, various lengths of human *ZFHX3*-promoter regions were cloned into pBluescriptIIKS(+) (Agilent Technologies – Stratagene Products, USA) with *Sal*I and *Bam*HI. The *Bss*HII and *Bam*HI fragments containing *ZFHX3* promoter regions were subcloned into the 5′ prime position of the luciferase gene of pGV-B basic vector (Toyo Ink, Japan) between *Mlu*I and *Bgl*II sites. The CRE site in 1.0 kbp of the *ZFHX3* promoter was mutagenized by PCR-based site-directed mutagenesis using a pair of primers, pGV-F (a forward primer with 5′ flanking sequence of luciferase gene on pGV-B): 5′-CAATGTATCTTATGGTACTG-3′, mCRE-R (a reverse direction at CRE site to introduce mutations): 5′-CGGAAATGACCACAGCAAAG-3′, mCRE-F (a forward direction primer at CRE site introduce mutations overlapped with mCRE-F): 5′-CTTTGCTGTGGTCATTTCCG-3′, pGV-R1 (a reverse primer including the first ATG codon of luciferase gene on pGV-B): 5′-CTTTATGTTTTTGGCGTCTTCC-3′, pGV-R2 (a reverse primer at 35-bp downstream from the pGV-R1 in luciferase gene on pGV-B): 5′-CCATCCTCTAGAGGATAGAATG-3′, to mutate the CRE site from 5′-TGACGTCA-3′ to 5′-TGTGGTCA-3′ (supplementary material Fig. S1). The two sets of PCR product were prepared with pGV-F and mCRE-R as a set, and mCRE-F and pVG-R2 as another set. These overlapping primary products were denatured together and reamplified with a new set of primers with pGV-F and pGV-R1. Reamplified products were trimmed with *Mlu*I and *Hin*dIII, and were subcloned into the same cloning site on the pGV-B basic vector. The CREB dominant-negative expression vector pCMV-CREB133 was from Clontech (USA; Cat. No. 631925).

Immunohistochemistry

Sections of 4 μm from 4% paraformaldehyde (PFA)-fixed, paraffin-embedded tissue were used. Tissue sections were deparaffinized and rehydrated and then both those for ZFHX3 (110°C, pressure cooker) and those for ATM (98°C, microwave oven) immunostaining were heated in citrate buffer (0.01 M, pH 6.0). The heat retrieval step was not applied for PDFGRB. Staining was carried out at room temperature. All sections were incubated with methanol containing 0.3% hydrogen peroxide and 1.0% sodium azide to block endogenous peroxidase activity, then incubated with mouse monoclonal anti-ATM Ser1981 phosphorylation site (pS-ATM) monoclonal antibody (at 1:1200 dilution: 7C10D8; Rockland, USA) followed by incubation with horseradish peroxidase (HRP)-conjugated anti-mouse IgG antibody (Envision labeled polymer, Dako Cytomation, Denmark), rabbit polyclonal anti-ZFHX3 antibody (at 1:50 dilution: D1-120; MBL, Nagoya, Japan) followed by HRP-conjugated anti-rabbit IgG antibody (Envision labeled polymer, Dako Cytomation, Denmark) or goat polyclonal anti-mouse PDGFRβ antibody (at 1:100 dilutions: R&D Systems, USA) followed by HRP-conjugated anti-goat IgG antibody [MAX-PO (G), Nichirei, Japan]. Primary antibodies and secondary antibodies were incubated at room for 1 hour. Immunoreactive products were then visualized after adding diaminobenzidine as a chromogen. BrdU labeling and detection was performed using a kit from Roche as per the manufacturer's recommendations. Tissue sections were counterstained with hematoxylin.

Immunocytochemistry

Cells were fixed in 4% PFA in PBS at room temperature for 20 minutes, then washed with 0.25% Triton-X in PBS, and blocked with 10% normal goat serum. Cells were then incubated for 1 hour at room temperature with primary antibodies against rabbit polyclonal anti-ZFHX3 antibody (at 1:100 dilution: D1-120; MBL, Japan), mouse monoclonal anti β-tubulin isotype III (at 1:500 dilution: 3D10; Sigma, USA), monoclonal anti-ATM Ser1981 phosphorylation site (pS-ATM) (at 1:100 dilution: 10H11.E12; Rockland, USA), rabbit polyclonal anti-γH2AX (at 1:100 dilution: BETHYL, USA). After three washes with 0.25% Triton-X in PBS, cells were visualized by secondary antibodies – Alexa-Fluor-488-conjugated goat anti-mouse for mouse monoclonal antibodies and Alexa-Fluor-546-conjugated goat anti-rabbit (at 1:1000 dilution; Molecular Probes, Invitrogen, USA) for rabbit polyclonal antibodies for 1 hour in the dark and, after two washes with PBS, nuclei were stained with 2.0 μg/ml DAPI (at 1:500 dilution of 1 mg/ml solution: 4′,6-diamino-2-phenylindole; Wako, Japan) for 5 minutes.

Western blotting

Cells were washed with washing buffer (10 mM 0.1 M phosphate buffer, 250 mM sucrose, 50 mM NaF), and total cell lysate was prepared with TNE buffer [20 mM Tris-HCl (pH 7.4), 150 mM NaCl, 2 mM EDTA, 1% Nonident-P40, 50 mM NaF]. The proteins were incubated on ice for 15 minutes, and then centrifuged at 15,000 ***g*** for 30 minutes at 4°C. The supernatant was obtained and stored at −80°C. The total protein content was measured using the Bradford Assay (Bio-Rad, Hercules, CA). For protein detection, each sample was separated on a 5-20% polyacrylamide gradient gel and the proteins were transferred to a polyvinylidene difluoride (PVDF) membrane (Millipore, Billerica, MA). The membrane was blocked with 3% BSA in Tris-buffered saline containing 0.05% Tween 20 (TBS-T) for 1 hour, washed in TBS-T, and then incubated for 1 hour at room temperature with primary antibodies for mouse monoclonal anti-α-tubulin (at 1:8000 dilution: B-5-1-2; Sigma, USA), rabbit polyclonal anti-ZFHX3 (at 1:2000 dilution: AT-6; MBL, Japan), mouse monoclonal anti-HA-tag (at 1:500 dilution: 5D8; MBL, Japan), mouse monoclonal anti-ATM (at 1:200 dilution: 5C2; Santa Cruz, USA), mouse monoclonal anti-pS-ATM (at 1:1000 dilution: 10H11.E12; Rockland, USA), goat polyclonal anti-PDGFRB (at 1:1000 dilution: R&D Systems, USA) or rabbit polyclonal anti-caspase 3 (at 1:1000 dilution: AAP-113; Assay Designs, USA). After washing in TBS-T, the membrane was incubated with peroxidase-conjugated anti-mouse IgG [at 1:10,000 dilution: anti-mouse IgG (H+L chain)-HRP; MBL, Japan] for mouse monoclonal antibodies, anti-rabbit IgG [at 1:5000 dilution: anti-rabbit IgG (H+L chain)-HRP, MBL, Japan] for rabbit polyclonal antibodies or anti-goat IgG [at 1:5000 dilution: anti-goat IgG (H+L chain)-HRP; MBL, Japan] for a goat polyclonal antibody for 1 hour at room temperature and washed in TBS-T. Immunoreactive signals were visualized by Amersham ECL Plus western blotting detection reagents (GE Healthcare, UK).

RNA extraction and RT-PCR analysis

Total RNA from cells was isolated using Trizol reagent (Invitrogen, USA), and 1 μg of total RNA was transcribed into cDNA using the Ready-To-Go You-Prime First-Strand Beads kit (GE Healthcare, UK). Real-time PCR was carried out with qPCR MasterMix Plus for SYBR Green (Eurogentec, USA) using the company's manual procedure: incubation at 95°C for 10 minutes followed by 40 cycles amplification (15 seconds at 95°C, 1 minute at 60°C, 45 seconds at 72°C and 15 seconds at 80°C) for SYBR Green detection. The primers used for real-time measurement of PCR were as follows: *Gapdh*, 5′-TGTGTCCGTCGTGGATCTGA-3′ and 5′-CCTGCTTCACCACCTTCTTGA-3′; *Zfhx3*, 5′-TTCTTTTCCTCCTCTCTCCTCATC-3′ and 5′-CGGTCCGTCGGACTTTTG-3′; *Col3a1*, 5′-GCACAGCAGTCCAACGTAGA-3′ and 5′-TCTCCAAATGGGATCTCTGG-3′); *Itga8*, 5′-AGTGGGAGGACCTGGAAGTT-3′ and 5′-AGTGGGAGGACCTGGAAGTT-3′; *Pdfgrb*, 5′-AACCCCCTTACAGCTGTCCT-3′ and 5′-TAATCCCGTCAGCATCTTCC-3′. The expression of each gene was normalized by the corresponding amount of *Gapdh* mRNA. The relative amounts of each product were calculated using the comparative CT (2-Δ Δ CT) method described in User Bulletin #2 of the ABI Prism 7500 fast Sequence Detection System (Applied Biosystems, USA).

TRANSLATIONAL IMPACT

Clinical issue

Ataxia telangiectasia (A-T) is a rare, recessive, neurodegenerative disease, with symptoms that normally appear in early childhood. Initial indications are usually ataxia (a lack of muscle control leading to loss of balance and coordination) and telangiectasia (tiny red veins, which are most noticeable on the whites of the eyes). The most serious clinical problem is loss of Purkinje cells, leading to degeneration of the cerebellum (the body's motor control centre). About 70% of sufferers also have thymic hypoplasia and a compromised immune system. Patients are also highly sensitive to X-irradiation and are susceptible to malignant tumors. Currently, there is no cure, nor any treatment that halts the progression of the disease.

A-T is caused by mutation of the *ATM* gene, which encodes a ubiquitous 370-kD serine-threonine kinase that is essential for normal repair of double-stranded DNA breaks; loss of ATM function results in DNA instability. However, there are atypical cases of A-T in which ATM is completely lacking: in these cases, DNA repair is defective, but symptoms are mild. These cases suggest that the severity of the neurological component of A-T might be due to a combination of defects, some of which are unknown.

Results

ATM phosphorylates several hundred substrates, including the transcription factor ZFHX3 (also known as ATBF1). In this study, the authors show that ZFHX3 is indirectly induced by ATM, and that ZFHX3 in turn induces the membrane tyrosine kinase PDGFRB, which is a survival factor in neurons. Neurons are highly susceptible to oxidative stress owing to their high rate of oxidative metabolism and low levels of antioxidant enzymes, and, in A-T mutant mice, oxidative stress is one of the major causes of Purkinje cell death. Inhibition of PDGFRB activity results in loss of ATM activity under conditions of oxidative stress, but not genotoxic stress, suggesting a means whereby ATM can rapidly autoregulate its activity.

To induce oxidative stress, mice were treated with kainic acid, resulting in predominantly cytoplasmic activation of ATM in the cerebral cortex, hippocampus and deep cerebellar nuclei (DCN). The authors propose that activation of ATM in the cytoplasm might play a role in autophagic protection of neurons against oxidative stress.

Implications and future directions

The signaling pathway from ATM to PDGFRB described here might be important in determining the response of neurons to oxidative stress, and be one of the hitherto unknown factors contributing to A-T. Therefore, targeting the action of PDGFRB might yield therapies that protect neurons against oxidative stress. The use of kainic acid to induce neuronal stress in mouse brains will also mean that *Atm*-deficient mice can be used to observe the early onset of neurodegeneration in the cerebellum; currently, the mice cannot be used as a model, because they die of cancer within 3-4 months, before manifestation of neurodegenerative disease. Kainic acid treatment will therefore be a good experimental tool to speed up screening of effective therapeutics.

doi:10.1242/dmm.006353

RNA interference

RNA interference (RNAi) was performed using Stealth/siRNA (Invitrogen, USA) duplex oligoribonucleotides against *Zfhx3* (*ATBF1*) (5′-UACACUGGUCAGACCACUGUCCUUG-3′ and 5′-CAAGGACAGUGGUCUGACCAGUGUA-3′), and three sets of duplex oligoribonucleotides against *Atm* (5′-UGAACUUCCCGAUAAUCCACAAGG-3′ and 5′-CCCUUGUGGAUUAUCAGGAAGUUCA-3′; 5′-UAAACAGAGAGAUACUUUCUCCUGC-3′ and 5′-GCAGGAGAAAGUAUCUCUCUGUUUA-3′; 5′-UUAGAAGGCCCACUUCCUCUUUGGC-3′ and 5′-GCCAAAGAGGAAGUGGGCCUUCUAA-3′). The transfection

was performed with Lipofectamine RNAiMAX four times to P19 cells during the neuronal differentiation process on days 0, 1, 3 and 5. Stealth RNAi negative control duplex (medium GC duplex) was also transfected four times, following the protocol of neuronal differentiation of P19 cells (Rudnicki and McBurney, 1987).

Statistics

Statistical analysis of results from luciferase assays and western blotting was performed using the Mann-Whitney U-test with Bonferroni Correction. All values were depicted as mean ± s.e.m. from at least three independent experiments and considered significant if $*P<0.01$. All the results from RT-PCR were normalized by the expression levels of *Gapdh* and compared as the increased ratio from control levels. Statistical significance was assessed with Student's *t*-test: $**P<0.001$.

ACKNOWLEDGEMENTS

We thank Yuji Fujinawa, Osamu Yamamoto and John Luff for excellent technical assistance, and Masaaki Inoue and Koichi Tsuneyama for scientific discussions. This study was supported by: a Grant-in-Aid for Special Research from Nagoya City University (Y.M.); a Grant-in-Aid for Exploratory Research (Y.M.); a Grant-in-Aid for Scientific Research [C] (M.K.) from Ministry of Education, Culture, Sports, Science and Technology of Japan; a Grant-in-Aid from The New Energy and Industrial Technology Development Organization of Japan (Y.M.); and a Grant-in-Aid from Japan Science and Technology Agency (Y.M.).

COMPETING INTERESTS

The authors declare no competing interests.

AUTHOR CONTRIBUTIONS

T.-S.K. and Y.M. contributed to all aspects of the project. M.S. performed the luciferase analysis. M.K. did pathological investigations. M.F.L. supplied brain samples of *Atm*-knockout mice. K.K.K. provided intellectual input and contributed towards writing of the manuscript. Y.S. operated the X-ray machine. C.-G.J. and K.A. provided comments on the manuscript. All investigators contributed to and reviewed the final report.

SUPPLEMENTARY MATERIAL

Supplementary material for this article is available at
http://dmm.biologists.org/lookup/suppl/doi:10.1242/dmm.004689/-/DC1

Received 17 October 2009; Accepted 11 July 2010.

REFERENCES

Alexander, A., Cai, S. L., Kim, J., Nanez, A., Sahin, M., MacLean, K. H., Inoki, K., Guan, K. L., Shen, J., Person, M. D. et al. (2010). ATM signals to TSC2 in the cytoplasm to regulate mTORC1 in response to ROS. *Proc. Natl. Acad. Sci. USA* **107**, 4153-4158.

Alterman, N., Fattal-Valevski, A., Moyal, L., Crawford, T. O., Lederman, H. M., Ziv, Y. and Shiloh, Y. (2007). Ataxia-telangiectasia: mild neurological presentation despite null ATM mutation and severe cellular phenotype. *Am. J. Med. Genet* **143A**, 1827-1834.

Andrews, P. W. (1984). Retinoic acid induces neuronal differentiation of a cloned human embryonal carcinoma cell line in vitro. *Dev. Biol.* **103**, 285-293.

Andrews, P. W., Damjanov, I., Simon, D., Banting, G. S., Carlin, C., Dracopoli, N. C. and Føgh, J. (1984). Pluripotent embryonal carcinoma clones derived from the human teratocarcinoma cell line Tera-2. Differentiation in vivo and in vitro. *Lab. Invest.* **50**, 147-162.

Bakkenist, C. J. and Kastan, M. B. (2003). DNA damage activates ATM through intermolecular autophosphorylation and dimer dissociation. *Nature* **421**, 499-506.

Banin, S., Moyal, L., Shieh, S., Taya, Y., Anderson, C. W., Chessa, L., Smorodinsky, N. I., Prives, C., Reiss, Y., Shiloh, Y. et al. (1998). Enhanced phosphorylation of p53 by ATM in response to DNA damage. *Science* **281**, 1674-1677.

Barlow, C., Hirotsune, S., Paylor, R., Liyanage, M., Eckhaus, M., Collins, F., Shiloh, Y., Crawley, J. N., Ried, T., Tagle, D. et al. (1996). Atm-deficient mice: a paradigm of ataxia telangiectasia. *Cell* **86**, 159-171.

Benjamin, E. J., Rice, K. M., Arking, D. E., Pfeufer, A., van Noord, C., Smith, A. V., Schnabel, R. B., Bis, J. C., Boerwinkle, E., Sinner, M. F. et al. (2009). Variants in ZFHX3 are associated with atrial fibrillation in individuals of European ancestry. *Nat. Genet.* **41**, 879-881.

Boehrs, J. K., He, J., Halaby, M. J. and Yang, D. Q. (2007). Constitutive expression and cytoplasmic compartmentalization of ATM protein in differentiated human neuron-like SH-SY5Y cells. *J. Neurochem.* **100**, 337-345.

Brooks, P. J., Wise, D. S., Berry, D. A., Kosmoski, J. V., Smerdon, M. J., Somers, R. L., Mackie, H., Spoonde, A. Y., Ackerman, E. J., Coleman, K. et al. (2000). The oxidative DNA lesion 8,5'-(S)-cyclo-2'-deoxyadenosine is repaired by the nucleotide excision repair pathway and blocks gene expression in mammalian cells. *J. Biol. Chem.* **275**, 22355-22362.

Burgner, D., Davila, S., Breunis, W. B., Ng, S. B., Li, Y., Bonnard, C., Ling, L., Wright, V. J., Thalamuthu, A., Odam, M. et al. (2009). A genome-wide association study identifies novel and functionally related susceptibility Loci for Kawasaki disease. *PLoS Genet.* **5**, e1000319.

Cheah, K. S., Stoker, N. G., Griffin, J. R., Grosveld, F. G. and Solomon, E. (1985). Identification and characterization of the human type II collagen gene (COL2A1). *Proc. Natl. Acad. Sci. USA* **82**, 2555-2559.

Chen, K., Albano, A., Ho, A. and Keaney, J. F., Jr (2003). Activation of p53 by oxidative stress involves platelet-derived growth factor-beta receptor-mediated ataxia telangiectasia mutated (ATM) kinase activation. *J. Biol. Chem.* **278**, 39527-39533.

Chen, P., Peng, C., Luff, J., Spring, K., Watters, D., Bottle, S., Furuya, S. and Lavin, M. F. (2003). Oxidative stress is responsible for deficient survival and dendritogenesis in purkinje neurons from ataxia-telangiectasia mutated mutant mice. *J. Neurosci.* **23**, 11453-11460.

Cho, Y. G., Song, J. H., Kim, C. J., Lee, Y. S., Kim, S. Y., Nam, S. W., Lee, J. Y. and Park, W. S. (2007). Genetic alterations of the ATBF1 gene in gastric cancer. *Clin. Cancer Res.* **13**, 4355-4359.

Coyle, J. T. and Puttfarcken, P. (1993). Oxidative stress, glutamate, and neurodegenerative disorders. *Science* **262**, 689-695.

Dupre, A., Boyer-Chatenet, L. and Gautier, J. (2006). Two-step activation of ATM by DNA and the Mre11-Rad50-Nbs1 complex. *Nat. Struct. Mol. Biol.* **13**, 451-457.

Fernandes, N. D., Sun, Y. and Price, B. D. (2007). Activation of the kinase activity of ATM by retinoic acid is required for CREB-dependent differentiation of neuroblastoma cells. *J. Biol. Chem.* **282**, 16577-16584.

Gorodetsky, E., Calkins, S., Ahn, J. and Brooks, P. J. (2007). ATM, the Mre11/Rad50/Nbs1 complex, and topoisomerase I are concentrated in the nucleus of Purkinje neurons in the juvenile human brain. *DNA Rep.* **6**, 1698-1707.

Gudbjartsson, D. F., Holm, H., Gretarsdottir, S., Thorleifsson, G., Walters, G. B., Thorgeirsson, G., Gulcher, J., Mathiesen, E. B., Njolstad, I., Nyrnes, A. et al. (2009). A sequence variant in ZFHX3 on 16q22 associates with atrial fibrillation and ischemic stroke. *Nat. Genet.* **41**, 876-878.

Ishii, Y., Oya, T., Zheng, L., Gao, Z., Kawaguchi, M., Sabit, H., Matsushima, T., Tokunaga, A., Ishizawa, S., Hori, E. et al. (2006). Mouse brains deficient in neuronal PDGF receptor-beta develop normally but are vulnerable to injury. *J. Neurochem.* **98**, 588-600.

Jung, C. G., Kim, H. J., Kawaguchi, M., Khanna, K. K., Hida, H., Asai, K., Nishino, H. and Miura, Y. (2005). Homeotic factor ATBF1 induces the cell cycle arrest associated with neuronal differentiation. *Development* **132**, 5137-5145.

Kao, F. T., Hawkins, J. W., Law, M. L. and Dugaiczyk, A. (1982). Assignment of the structural gene coding for albumin to human chromosome 4. *Hum. Genet.* **62**, 337-341.

Kataoka, H., Miura, Y., Joh, T., Seno, K., Tada, T., Tamaoki, T., Nakabayashi, H., Kawaguchi, M., Asai, K., Kato, T. et al. (2001). Alpha-fetoprotein producing gastric cancer lacks transcription factor ATBF1. *Oncogene* **20**, 869-873.

Khanna, K. K. and Jackson, S. P. (2001). DNA double-strand breaks: signaling, repair and the cancer connection. *Nat. Genet.* **27**, 247-254.

Kim, C. J., Song, J. H., Cho, Y. G., Cao, Z., Lee, Y. S., Nam, S. W., Lee, J. Y. and Park, W. S. (2008). Down-regulation of ATBF1 is a major inactivating mechanism in hepatocellular carcinoma. *Histopathology* **52**, 552-559.

Kuljis, R. O., Chen, G., Lee, E. Y., Aguila, M. C. and Xu, Y. (1999). ATM immunolocalization in mouse neuronal endosomes: implications for ataxia-telangiectasia. *Brain Res.* **842**, 351-358.

Lein, E. S., Hawrylycz, M. J., Ao, N., Ayres, M., Bensinger, A., Bernard, A., Boe, A. F., Boguski, M. S., Brockway, K. S., Byrnes, E. J. et al. (2007). Genome-wide atlas of gene expression in the adult mouse brain. *Nature* **445**, 168-176.

Li, J., Han, Y. R., Plummer, M. R. and Herrup, K. (2009). Cytoplasmic ATM in neurons modulates synaptic function. *Curr. Biol.* **19**, 2091-2096.

Marshall, H., Morrison, A., Studer, M., Popperl, H. and Krumlauf, R. (1996). Retinoids and Hox genes. *FASEB J.* **10**, 969-978.

Matsuoka, S., Ballif, B. A., Smogorzewska, A., McDonald, E. R., 3rd, Hurov, K. E., Luo, J., Bakalarski, C. E., Zhao, Z., Solimini, N., Lerenthal, Y. et al. (2007). ATM and ATR substrate analysis reveals extensive protein networks responsive to DNA damage. *Science* **316**, 1160-1166.

Miura, Y., Tam, T., Ido, A., Morinaga, T., Miki, T., Hashimoto, T. and Tamaoki, T. (1995). Cloning and characterization of an ATBF1 isoform that expresses in a neuronal differentiation-dependent manner. *J. Biol. Chem.* **270**, 26840-26848.

Miura, Y., Kataoka, H., Joh, T., Tada, T., Asai, K., Nakanishi, M., Okada, N. and Okada, H. (2004). Susceptibility to killer T cells of gastric cancer cells enhanced by Mitomycin-C involves induction of ATBF1 and activation of p21 (Waf1/Cip1) promoter. *Microbiol. Immunol.* **48**, 137-145.

Morinaga, T., Yasuda, H., Hashimoto, T., Higashio, K. and Tamaoki, T. (1991). A human alpha-fetoprotein enhancer-binding protein, ATBF1, contains four homeodomains and seventeen zinc fingers. *Mol. Cell. Biol.* **11**, 6041-6049.

Narendra, D., Tanaka, A., Suen, D. F. and Youle, R. J. (2008). Parkin is recruited selectively to impaired mitochondria and promotes their autophagy. *J. Cell Biol.* **183**, 795-803.

Olney, J. W., Rhee, V. and Ho, O. L. (1974). Kainic acid: a powerful neurotoxic analogue of glutamate. *Brain Res.* **77**, 507-512.

Reuterdahl, C., Sundberg, C., Rubin, K., Funa, K. and Gerdin, B. (1993). Tissue localization of beta receptors for platelet-derived growth factor and platelet-derived growth factor B chain during wound repair in humans. *J. Clin. Invest.* **91**, 2065-2075.

Rudnicki, M. A. and McBurney, M. W. (1987). Cell culture methods and induction of differentiatin of embryonal carcinoma cell lines. In *Teratocarcinomas and Embryonic Stem Cells a Practical Approach* (ed. E. J. Robertson), pp. 14-49. Oxford, Washington DC: IRL Press.

Savitsky, K., Bar-Shira, A., Gilad, S., Rotman, G., Ziv, Y., Vanagaite, L., Tagle, D. A., Smith, S., Uziel, T., Sfez, S. et al. (1995). A single ataxia telangiectasia gene with a product similar to PI-3 kinase. *Science* **268**, 1749-1753.

Shi, Y., Venkataraman, S. L., Dodson, G. E., Mabb, A. M., LeBlanc, S. and Tibbetts, R. S. (2004). Direct regulation of CREB transcriptional activity by ATM in response to genotoxic stress. *Proc. Natl. Acad. Sci. USA* **101**, 5898-5903.

Shieh, S. Y., Ikeda, M., Taya, Y. and Prives, C. (1997). DNA damage-induced phosphorylation of p53 alleviates inhibition by MDM2. *Cell* **91**, 325-334.

Shiloh, Y. (2003). ATM and related protein kinases: safeguarding genome integrity. *Nat. Rev. Cancer* **3**, 155-168.

Sun, X., Frierson, H. F., Chen, C., Li, C., Ran, Q., Otto, K. B., Cantarel, B. L., Vessella, R. L., Gao, A. C., Petros, J. et al. (2005). Frequent somatic mutations of the transcription factor ATBF1 in human prostate cancer. *Nat. Genet.* **37**, 407-412.

Urano, Y., Sakai, M., Watanabe, K. and Tamaoki, T. (1984). Tandem arrangement of the albumin and alpha-fetoprotein genes in the human genome. *Gene* **32**, 255-261.

Wang, Y., Han, R., Liang, Z. Q., Wu, J. C., Zhang, X. D., Gu, Z. L. and Qin, Z. H. (2008). An autophagic mechanism is involved in apoptotic death of rat striatal neurons induced by the non-N-methyl-D-aspartate receptor agonist kainic acid. *Autophagy* **4**, 214-226.

Wilkinson, D. S., Tsai, W. W., Schumacher, M. A. and Barton, M. C. (2008). Chromatin-bound p53 anchors activated Smads and the mSin3A corepressor to confer transforming-growth-factor-beta-mediated transcription repression. *Mol. Cell. Biol.* **28**, 1988-1998.

Yasuda, H., Mizuno, A., Tamaoki, T. and Morinaga, T. (1994). ATBF1, a multiple-homeodomain zinc finger protein, selectively down-regulates AT-rich elements of the human alpha-fetoprotein gene. *Mol. Cell. Biol.* **14**, 1395-1401.

Zemskov, E. A., Loukinova, E., Mikhailenko, I., Coleman, R. A., Strickland, D. K. and Belkin, A. M. (2009). Regulation of platelet-derived growth factor receptor function by integrin-associated cell surface transglutaminase. *J. Biol. Chem.* **284**, 16693-16703.

Zhang, J., Zhang, D., McQuade, J. S., Behbehani, M., Tsien, J. Z. and Xu, M. (2002). c-fos regulates neuronal excitability and survival. *Nat. Genet.* **30**, 416-420.

Honokiol Increases ABCA1 Expression Level by Activating Retinoid X Receptor Beta

Cha-Gyun JUNG,*[,a] Hirofumi HORIKE,[a,#] Byung-Yoon CHA,[b] Kyung-Ok UHM,[a] Rena YAMAUCHI,[a] Takamasa YAMAGUCHI,[a] Takashi HOSONO,[a] Kagami IIDA,[b] Je-Tae WOO,[b] and Makoto MICHIKAWA*[,a]

[a] *Department of Alzheimer's Disease Research, Research Institute, National Center for Geriatrics and Gerontology (NCGG); 35 Morioka, Obu, Aichi 474–8522, Japan: and* [b] *Research Institute for Biological Functions, Chubu University; 1200 Matsumoto, Kasugai, Aichi 488–8501, Japan.*

Received March 2, 2010; accepted April 14, 2010; published online April 20, 2010

ABCA1, a member of the ATP-binding cassette transporter family, regulates high-density lipoprotein (HDL) metabolism and reverses cholesterol transport. Its expression is upregulated mainly by the activation of the liver X receptor (LXR), retinoid X receptor (RXR), and peroxisome proliferator-activated receptors (PPARs). To identify natural compounds that can upregulate ABCA1 expression, we developed a reporter assay using U251-MG (human glioma cell line) cells that stably express a human ABCA1 promoter-luciferase and performed a cell-based high-throughput screening of 118 natural compounds. Using this system, we identified honokiol, a compound extracted from *Magnolia officinalis*, as an activator of the ABCA1 promoter. We found that honokiol also increased ABCA1 mRNA and protein expression levels in a dose-dependent manner in U251-MG cells without significant cell death and also increased ABCA1, ABCG1 and apolipoprotein E (apoE) expression levels in THP-1 macrophages. PPAR antagonists did not diminish the induction of ABCA1 expression by honokiol in U251-MG cells. Cotreatment of the cells with honokiol and T0901317 (synthetic LXR ligand) further increased the ABCA1 expression level, whereas cotreatment with 9-*cis* retinoic acid had no additive effect compared with treatment with honokiol alone. We also found that honokiol has binding affinity to RXRβ. In this study, we identified for the first time honokiol as an upregulator of ABCA1 expression, which is mediated by the binding of honokiol to RXRβ as a ligand.

Key words ATP-binding cassette transporter 1; cell-based assay; honokiol; liver X receptor; retinoid X receptor; peroxisome proliferator-activated receptor

ABCA1, a member of the ATP-binding cassette transporter family, promotes the efflux of cholesterol and phospholipids from intracellular compartments to extracellular cholesterol acceptors.[1] Mutations in the ABCA1 gene result in high-density lipoprotein (HDL) deficiency syndromes, such as Tangier disease, which is characterized by low levels of HDL cholesterol and apolipoprotein A—I (apoA—I) and an increased risk of cardiovascular disease.[2,3] ABCA1 also plays an important role in the central nervous system (CNS). Apolipoprotein E (apoE) is one of the major apolipoproteins in CNS, which interacts with ABCA1[4] to remove cholesterol from cells and generates HDL particles in the cerebrospinal fluid.[5] The lack of ABCA1 results in a reduction of apoE levels and lipidated apoE-containing lipoproteins in the brain of ABCA1$^{-/-}$ mice.[6] It has also been reported that decreased apoE levels and poorly lipidated apoE increase amyloid-β peptide (Aβ), a major component of the senile plaque in Alzheimer disease (AD) brains, deposition in ABCA1$^{-/-}$ mice crossed with the AD mouse model.[7] In contrast, overexpression of ABCA1 results in the reduction of Aβ deposition through ABCA1-mediated generation of apoE containing lipoproteins in the AD mouse model[8] suggesting that modulation of ABCA1 expression could be a possible therapeutic strategy for AD.

ABCA1 is ubiquitously expressed, the expression of which is transcriptionally regulated. The activation of liver X receptor (LXR) by oxysterols and the nonsteriodal synthetic LXR agonist T0901317 increases ABCA1 gene expression level.[9] ABCA1 is also regulated by peroxisome proliferator-activated receptors (PPARs) through their inductive effects on the expression of LXRα.[10] Both of these types of receptor form heterodimers with retinoid X receptors (RXRs),[11] and LXR/RXR and PPARs/LXR heterodimers bind to a promoter sequence on the ABCA1 gene.[10,12] In mice models, the synthetic LXR agonist GW3965 increases the plasma HDL cholesterol level and inhibits the development of atherosclerosis,[13] and decrease Aβ deposition in the AD mouse model.[14] Although ABCA1 plays an important role in the development of atherosclerosis and pathogenesis of AD, there are relatively few drugs that can upregulate ABCA1 expression. Thus, identification of upregulators of ABCA1 expression may lead to a therapeutic benefit for patients with cardiovascular disease and AD.

Because of their simplicity and sensitivity, reporter gene assay systems are used for high-throughput screening (HTS) to identify new compounds for drug development. These strategies offer the advantages of speed, cost-effectiveness, genome coverage, and immediate biological relevance. In the present study, we have developed an HTS method of identifying ABCA1 upregulators, and screened 118 natural compounds using the developed cell-based assay.

MATERIALS AND METHODS

Materials Honokiol and rosiglitazone were purchased from LKT laboratories, Inc. (St. Paul, MN, U.S.A.) and Cayman Chemical (Ann Arbor, MI, U.S.A.), respectively. GW6471, GW9662, T0901317 and 9-*cis*-retinoic acid (9CRA) were purchased from Sigma-Aldrich (St. Louis, MO, U.S.A.). All other reagents were purchased from Wako Pure Chemical Industries, Ltd. (Osaka, Japan).

Cell Cultures U251-MG cells were cultured in Dul-

* To whom correspondence should be addressed. e-mail: jung@ncgg.go.jp; michi@ncgg.go.jp
# Equal contribution with first author.

becco's modified Eagle's medium (DMEM) without antibiotics supplemented with 10% fetal bovine serum (FBS). Human THP-1 monocytes were purchased from the American Type Culture Collection (Manassas, VA, U.S.A.). To differentiate THP-1 cells into macrophages, the THP-1 cells were treated with 3.2×10^{-7} M phorbol 12-myristate 13-acetate (PMA) (Sigma-Aldrich) in the growth medium for 72 h. The differentiated THP-1 macrophages were cultured in RPMI 1640 medium, and 0.2% bovine serum albumin (BSA). Cerebral cortical neuron- and astrocyte-rich cultures were prepared from embryonic day 17 (E17) and postnatal 1 (P1) Sprague-Dawley rats, respectively, as described previously.[15] All the cells were cultured at 37 °C in a humidified 5% CO_2 incubator.

Reporter Plasmid Constructs and Preparation of Stable Cell Lines A 1214-bp fragment of the human ABCA1 promoter (−990/+224) was amplified by polymerase chain reaction (PCR) using the sense primer 5′-CCCCTCGAGTCCAGTGTTTTGGGTAGTTT-3′ with the *Xho*I site and the antisense primer 5′-CGCAAGCTTTTACCTGTTTTCCACTTTTG-3′ with *Hin*dIII site. The amplified PCR products were digested with *Xho*I and *Hin*dIII, then ligated into the pGL4.14 firefly luciferase reporter plasmid (Promega Corp., Madison, WI, U.S.A.) at the *Xho*I and *Hin*dIII sites to generate pGL4.14hABCA1p (for human ABCA1 promoter). The construct was confirmed by DNA sequencing. To generate stable U251-MG cell lines expressing human ABCA1 promoter-luciferase, the U251-MG cells seeded in 6-well plates at 7×10^4 cells/well were transfected with pGL4.14hABCA1p using FuGENE HD (Roche, Mannheim, Germany), followed by the selection of stable transfectants using 0.3 mg/ml hygromycin (Invitrogen Corp., Carlsbad, CA, U.S.A.) in the growth medium for 7 d.

High-Throughput Screening of Natural Compounds U251-MG/hABCA1p cells were seeded in 96-well plates at a density of 10000 cells/well in 100 μl of medium. After 24 h, 118 natural compounds were added at a final concentration of 10 μM in 0.1% dimethyl sulfoxide (DMSO) or vehicle control (0.1% DMSO, final concentration), and the cells were further incubated for 24 h. The luciferase activity was measured using the Luciferase Assay System (Promega) following the manufacturer's instructions and luciferase activity was measured using a GLOMAX 96-microplate Luminometer (Promega). All luciferase activity experiments were performed in duplicate. The statistical Z'-factor that can be used to evaluate the quality of the HTS assay was calculated.[16] The Z'-factor was determined using the formula $Z'=1-[(3\sigma_{c^+}+3\sigma_{c^-})/(\mu_{c^+}-\mu_{c^-})]$, where σ is the standard deviation, μ is the mean, c^+ is 9CRA treatment, and c^- is vehicle treatment (0.1% DMSO).

RNA Extraction and Real-Time PCR Total RNA was isolated from U251-MG cells, THP-1 macrophages and primary cortical neurons using an RNeasy plus mini kit (Qiagen, Valencia, CA, U.S.A.) following the manufacturer's instructions. Reverse transcription was performed from 1 μg of total RNA using the PrimeScript RT reagent kit (Takara, Japan). Real-time PCR was carried out using the SYBR Premix Ex *Taq* system and a Thermal Cycler Dice Real-Time System (Takara). The expression of each gene was normalized with the corresponding amount of actin mRNA using the comparative threshold cycle method following the manufacturer's protocols. Amplification was performed using the following primers (sense and antisense): human ABCA1 (5′-TTCGCTCTGAGATGAGCACCA-3′ and 5′-TTTCAAGCGGGCATAGAACCA-3′), human ABCG1 (5′-ACGCAGTTCTGCATCCTCTT-3′ and 5′-CGGAGTTGCTCAAGACCTTC-3′), human ApoE (5′-GGTCGCTTTTGGGATTACCT-3′ and 5′-CTCCAGTTCCGATTTGT-3′), rat ABCA1 (5′-GGTTTGGGGAGGAAATTGAT-3′ and 5′-AACCATCCACAGCAACCTTC-3′), and human and rat actin (5′-CATCCGTAAAGACCTCTATGCCAAC-3′ and 5′-ATGGAGCCACCGATCCACA-3′).

Western Blot The cells were washed with PBS and homogenized in lysis buffer (10 mM Tris–HCl (pH 7.4), 150 mM NaCl, 1 mM ethylenediaminetetraacetic acid (EDTA), 1% Triton-X) containing a protease inhibitor cocktail (Roche). The homogenates were rocked at 4 °C for 30 min and centrifuged at 20000×***g*** at 4 °C for 30 min to remove cell debris. The supernatant was collected and protein concentration was determined using a BCA protein assay kit (Pierce, Rockford, IL, U.S.A.). Equal amounts of protein were subjected to 7.5% or 5—20% gradient sodium dodecyl sulfate (SDS) polyacrylamide gels electrophoresis and transferred to polyvinylidene difluoride membrane (Millipore, Billerica, MA, U.S.A.). These membranes were then blocked with 5% skim milk in 10 mM Tris–HCl (pH 7.5), 150 mM NaCl, 0.1% Tween 20 for 1 h at room temperature or overnight at 4 °C. These membranes were incubated with primary antibodies, namely, anti-ABCA1 antibody (1 : 1000; Santa Cruz, CA, U.S.A.), anti-ABCG1 antibody (1 : 1500; Novus Biological, Cambridge, U.K.), anti-apoE antibody (1 : 1000; Chemicon, Temecula, CA, U.S.A.) or anti-actin antibody (1 : 2000; Sigma). The membranes were washed, followed by incubation with the appropriate secondary antibody-conjugated to horseradish peroxidase. Immunoreactive signals were visualized with ECL™ or ECL Plus™ Western blotting detection reagent (GE Healthcare, Piscataway, NJ, U.S.A.) and exposed to an LAS-3000 Mini Bio-imaging Analyzer System (FUJIFILM Co., Tokyo, Japan). The signal intensity was quantified using MultiGauge software (FUJIFILM).

TUNEL Assay Apoptosis was assessed by TUNEL (terminal deoxynucleotidyl transferase-mediated dUTP nick-end labeling) staining using an ApopTag Fluorescein Direct In Situ Apoptosis Detection Kit according to manufacturer's instructions (Chemicon). DNA fragmentation was evaluated in U251-MG cells following treatment with different concentrations of honokiol. Briefly, cells was fixed with 1% paraformaldehyde in PBS for 10 min at room temperature and permeabilized in EtOH : acetic acid (2 : 1) for 5 min at −20 °C. Cells were then washed with PBS and Fluorescein-conjugated nucleotide and TdT enzyme was added and incubated for 1 h at 37 °C. Nuclei were stained with DAPI.

Cell Viability Assay Cell viability was evaluated by WST-8 [2-(2-methoxy-4-nitrophenyl)-3-(4-nitrophenyl)-5-(2,4-disulfophenyl)-2*H*-tetrazolium, monosodium salt] colorimetric assay. U251-MG cells were treated with various concentrations of honokiol for 24 h. Then, 10 μl of WST-8 reagent (Cell Counting Kit, Dojindo Lab., Japan) was added and incubated for 2 h. Cell viability was determined following the manufacturer's instructions.

RXRβ Ligand Binding Assay For RXRβ ligand binding activity measurement, we used the Lanthascreen™ TR-

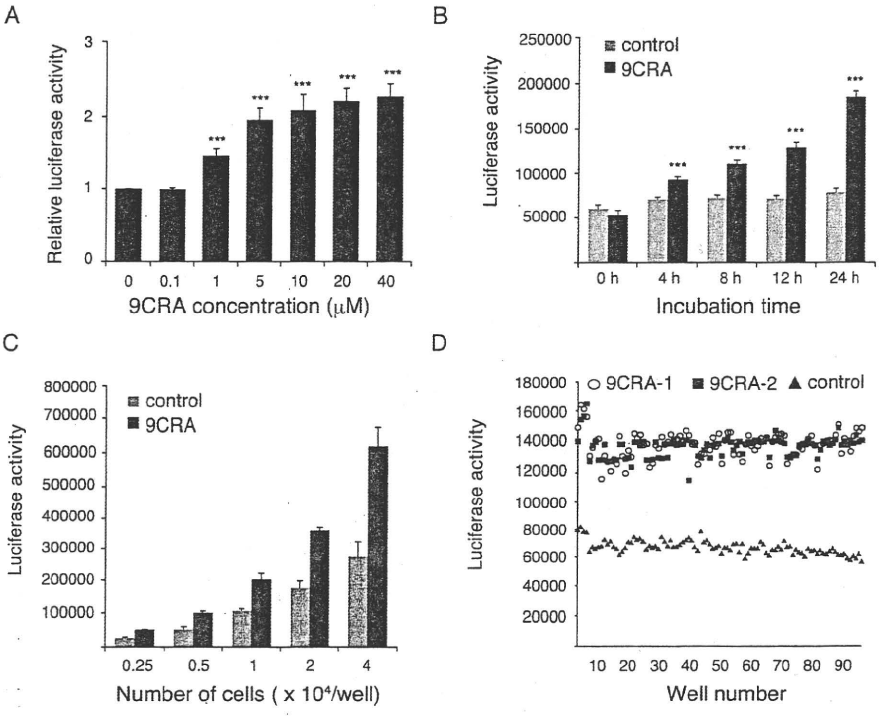

Fig. 1. (A) Effect of 9CRA on Activity of ABCA1 Promoter Reporter Gene

U251-MG/hABCA1p cell cells stably expressing human ABCA1 promoter-luciferase were seeded in 96-well plates at 10000 cells/well. After 24 h, the cells were treated with the indicated concentrations of 9CRA or vehicle control (0.1% DMSO) for 24 h, and the luciferase activity was measured.

(B) Effect of Incubation Time on Activity of ABCA1 Promoter Reporter Gene

U251-MG/hABCA1p cells seeded in 96-well plates at 10000 cells/well were incubated for indicated duration in the presence of 9CRA (10 μM), and the luciferase activity was measured.

(C) Effect of Cell Number on Activity of ABCA1 Promoter Reporter Gene

U251-MG/hABCA1p cells were seeded in 96-well plates at indicated cell numbers. After 24 h, the cells were treated with 9CRA (10 μM) for 24 h and the luciferase activity was measured.

(D) Analysis of Variability of Screening System

U251-MG/hABCA1p cells were seeded in 96-well plates at 10000 cells/well, cultured for 24 h, and treated with 9CRA (10 μM, positive control, two plates) or vehicle (0.1% DMSO, negative control, one plate) for another 24 h, and the luciferase activity was measured. The assay results from the two positive-control plates were combined and used to calculate the Z'-factor. All values are presented as mean±S.D. of three independent experiments. *** $p<0.001$ *vs.* control.

FRET RXRβ Coactivator Assay (Invitrogen). The LanthaScreen™ TR-FRET-based nuclear receptor coactivator recruitment assay uses a terbium (Tb)-labeled anti-GST antibody, a fluorescein-labeled coactivator peptide and RXRβ ligand-binding domain (RXRβ-LBD) tagged with glutathione-*S*-transferase (GST). Tb-anti-GST antibody indirectly labels the RXRβ-LBD by binding to the GST tag. Binding of the agonist to RXRβ LBD causes a conformational change that results in an increase in the affinity of the RXRβ for a coactivator peptide. The close proximity of the fluorescently labeled coactivator peptide to the Tb-labeled antibody causes an increase in the TR-FRET signal intensity. The TR-FRET ratio of 520/495 was calculated using an EnVision™ multi label reader (Perkin-Elmer. Inc., U.S.A.) with an excitation wavelength of 340 nm and emission wavelengths of 520 nm and 495 nm.

RESULTS AND DISCUSSION

Establishment of a Cell-Based Assay to Screen Upregulators of Human ABCA1 Promoter As an initial step to identify natural compounds that can upregulate ABCA1 expression, we developed a stable cell line expressing human ABCA1 promoter-luciferase (U251-MG/hABCA1p) as described in Materials and Methods. In this study, we used glioma cell line, U251-MG cells, because ABCA1 is expressed in astrocytes, and its expression increases markedly after exposure to oxysterols and 9CRA, which are ligands for LXR and RXR, respectively.[17] In our system, we also confirmed that 9CRA increased the luciferase activity in a dose-dependent manner in U251-MG cells (Fig. 1A). We also carried out two experiments to optimize the reporter gene assay. First, we examined the effect of incubation time on reporter gene assay in the absence or presence of 9CRA. Our results showed that approximately 24 h of incubation with 9CRA yielded the highest response (Fig. 1B). Second, we also examined the effect of the number of cells per well on reporter gene assay in the absence or presence of 9CRA. The luciferase activity of these cells increased gradually with increasing cell number in the absence or presence of 9CRA (Fig. 1C). 9CRA treatment increased the luciferase activity by two fold compared with the control regardless of cell number. Therefore, we used 24 h as the incubation time and 10000 cells/well in all our experiments. In addition, we also calculated the coefficient of variation (CV) for the assay in a 96-well plate. The CV values were 7.7% for vehicle-treated

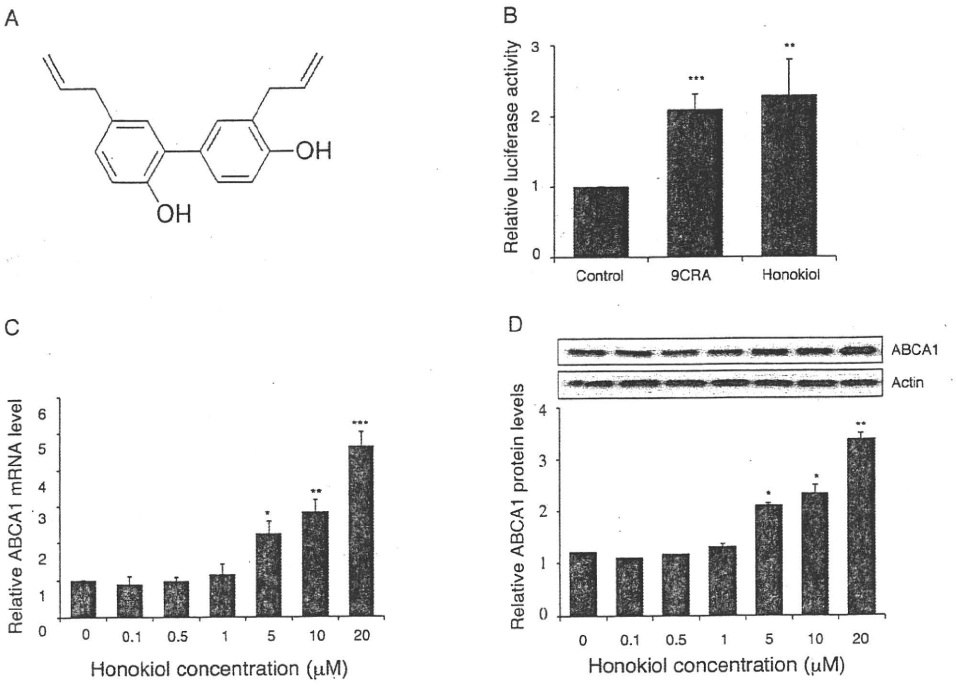

Fig. 2. Honokiol Increased the mRNA and Protein Levels of ABCA1 in U251-MG Cells

(A) Chemical structure of honokiol. U251-MG/hABCA1p cells were seeded in 96-well plates at 10000 cells/well. After 24 h, the cells were treated with 10 μM 9CRA, honokiol or vehicle control (0.1% DMSO) and cultured for 24 h. The cells were then harvested and used for the determination of luciferase activity (B), ABCA1 mRNA level (C), and ABCA1 protein level (D). (C) For determination of mRNA level, real-time PCR analysis was performed. The expression of ABCA1 mRNA was normalized with corresponding amount of actin mRNA and expressed as a value relative to the control. (D) For determination of expression levels of ABCA1 and actin, Western blotting using anti-ABCA1 and anti-actin antibodies was perfomred. A representative immunoblot is shown (upper panel), and bands were quantified by densitometry, normalized to actin, and expressed as a value relative to the control (lower graph).

cells and 5.4% for 9CRA-treated cells. The Z'-factor was 0.71 (Fig. 1D). These results indicate that the assay system could be used for HTS.

Honokiol Increased ABCA1 Expression Level without Significant Cell Death Using the cell-based reporter gene assay, we screened 118 natural compounds for their potential to activate ABCA1 gene promoter. Among the 118 compounds, we found that honokiol, a compound extracts from *Magnolia officinalis* (Fig. 2A), can increase the ABCA1 promoter activity by two fold compared with the vehicle control (Fig. 2B). Next, we confirmed the effect of honokiol on endogenous ABCA1 expression. Treatment of U251-MG cells with various concentrations of honokiol significantly increased ABCA1 mRNA (Fig. 2C) and protein expression levels (Fig. 2D) in a dose-dependent manner. Honokiol has a variety of biological effects, including antitumor and anti-angiogenic effects.[18,19] In addition, honokiol promotes neurite outgrowth by induction of the expression of neurotrophic factors such as NGF and BDNF in rat embryonic neurons.[20] In this study, we found that honokiol efficiently increased ABCA1 mRNA and protein levels, indicating that the honokiol-induced ABCA1 expression is transcriptinally regulated (Figs. 2C, D).

Given that ABCA1 expression is upregulated during apoptosis in human fibroblasts,[21] and honokiol induces apoptosis in tumor cells,[22] we also examined apoptotic processes by TUNEL assay, an indicator of cell death accompanied by DNA fragmentation, in U251-MG cells following the treatment with indicated concentrations (0, 10, 20, 80 μM) of honokiol. As shown in Fig. 3A, apoptotic induction was observed in cells treated with 80 μM of honokiol, whereas it was not observed up to 20 μM. Similarly, we found that honokiol treatment did not induce cell death up to 20 μM, but honokiol at concentrations of 40 and 80 μM induced cell death (Fig. 3B). Our results are consistent with those of other reports showing that over 40 μM honokiol decreases the viability of prostate cancer cells but has no effect at 20 μM.[22] The fact that the honokiol treatment at concentrations lower than 20 μM did not cause cell death indicates that the increased expression of ABCA1 due to honokiol is not a cause of cell death.

Enhanced ABCA1 Expression by Honokiol Is Mediated by RXR Activation ABCA1 expression is mainly regulated *via* the activation of PPARs/RXR and LXR/RXR. Therefore, we further investigated the potential mechanism by which honokiol increases the ABCA1 expression level. To determine whether honokiol can activate PPARs to increase the ABCA1 expression level, we examined the effect of PPAR antagonists on honokiol-induced ABCA1 expression in U251-MG cells. In these cells, the ABCA1 protein levels increased by honokiol were not diminished by the PPARα antagonist (GW6471) or PPARγ antagonist (GW9662) (Fig. 4A). These results indicate that the honokiol-induced ABCA1 expression is not a cause of the stimulation of PPARs by honokiol. We also examined the additive effect of 9CRA and T0901317 (synthetic LXR agonist) on the honokiol-induced ABCA1 expression. Combined treatment with honokiol and 9CRA did not change the ABCA1 protein levels, but the combination of honokiol and T0901317 resulted in increased ABCA1 protein levels compared with treatment

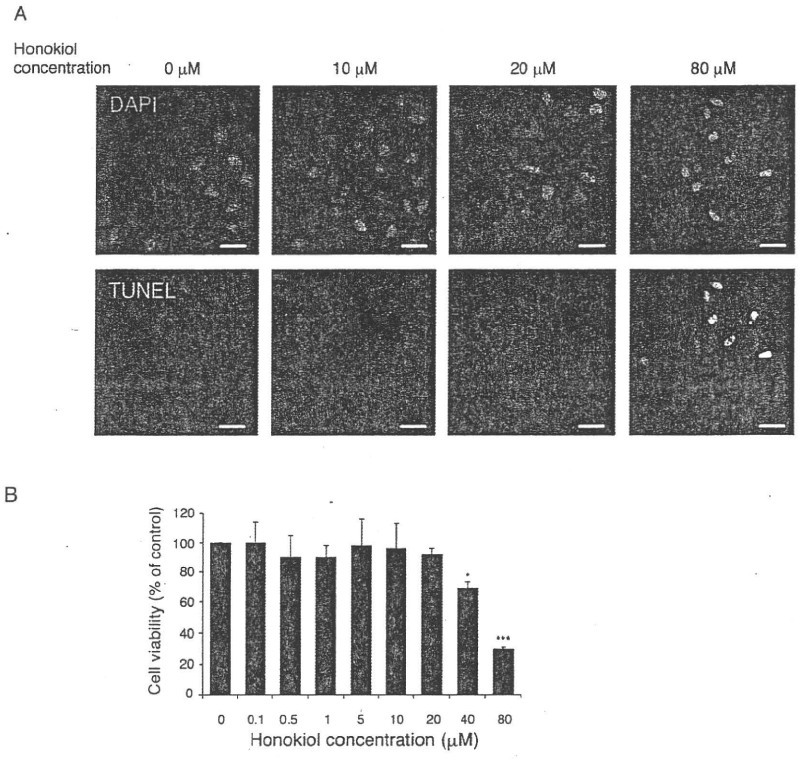

Fig. 3. Effect of Honokiol on Apoptosis (A) and Viability (B) of U251-MG Cells

(A) Apoptotic cells in U251-MG cells treated with indicated concentrations of honokiol for 24 h were detected by TUNEL staining. Nuclei were stained with DAPI. Representative of three experiments. Scale bar=25 μm. (B) Cell viability was determined using a cell counting kit (WST-8) and is shown as a percentage of living cells. All the values are presented as mean±S.D. of three independent experiments. * $p<0.05$, *** $p<0.001$ *vs.* control.

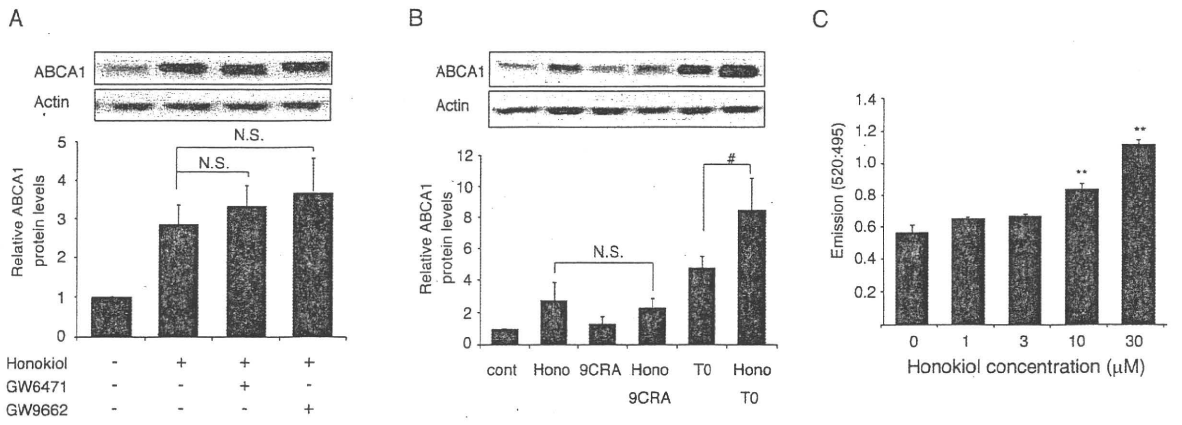

Fig. 4. Honokiol Induced ABCA1 Expression *via* Activation of RXRβ in U251-MG Cells

(A) Effects of PPARα antagonist GW6471 and PPARγ antagonist GW9662 on honokiol-induced ABCA1 expression. The cells were treated with 10 μM GW6471 or GW9662 for 1 h and subsequently treated for 24 h with or without honokiol (20 μM). The cells were lysed, and the protein expression levels of ABCA1 and actin were determined by Western blotting using anti-ABCA1 and anti-actin antibodies. (B) The cells were treated for 24 h with 10 μM 9CRA, T0901317 (T0), or vehicle control (cont) in the presence or absence of 20 μM honokiol (Hono). A representative immunoblot from three independent experiments is shown (upper panel) and the bands were quantified by densitometry, normalized to actin, and expressed as a value relative to the control (lower graph). (C) RXRβ ligand binding activity of honokiol. The binding affinity of honokiol towards the RXRβ LBD at the indicated concentrations of honokiol was measured using the Lanthascreen™ TR-FRET RXRβ Coactivator Assay. All values are presented as mean±S.D. of three independent experiments. ** $p<0.01$ *vs.* control. # $p<0.05$ *vs.* T0 treatment. N.S., not significant.

with honokiol alone (Fig. 4B). This combination of honokiol and T0901317 had a greater than additive effect. These results indicate that the honokiol-induced ABCA1 expression is mediated by RXR activation.

Honokiol Has RXRβ Ligand Binding Activity RXR has three subtypes, α, β, γ, which can form heterodimers with LXRs to induce ABCA1 expression. RXRβ heterodimerizes with LXRs to induce ABCA1 expression,[23] thus, we firstly examined whether honokiol serves as an RXRβ ligand. In the RXRβ binding assay, honokiol exhibited RXRβ affinities of 1.5- and 2-fold at 10 and 30 μM, respectively (Fig. 4C). This result indicates that honokiol activates RXRβ as a ligand, which, in turn, enhances ABCA1 expression. But further investigations are required to determine whether honokiol also binds to RXRα and RXRγ, because they can also heterodimerize with LXRs to induce

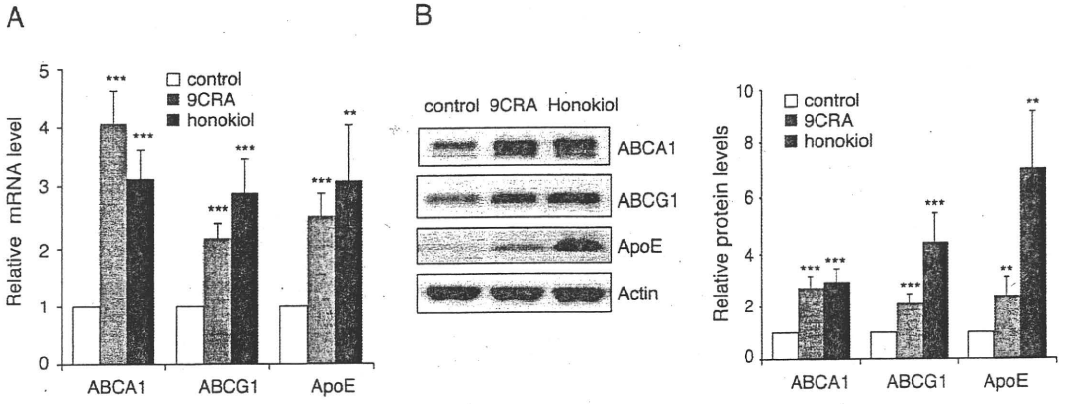

Fig. 5. Honokiol Increased the Expression Level of ABCA1, ABCG1 and apoE in THP-1 Macrophages

THP-1 cells were exposed for 72 h to phorbol 12-myristate 13-acetate (PMA) in RPMI 1640 containing 10% FBS to induce differentiation to macrophages. On day 4, THP-1 macrophages were treated for 24 h with 10 μM 9CRA, honokiol or vehicle control (0.1% DMSO) in RPMI 1640 medium containing 0.2% bovine serum albumin. (A) Total RNA was prepared from the cells and the mRNA expression of ABCA1, ABCG1 and apoE was measured by real-time PCR and expressed as a value relative to actin. (B) The protein levels of ABCA1, ABCG1 and apoE in whole lysates of THP-1 macrophages treated with 10 μM 9CRA, honokiol or vehicle control for 24 h were determined by Western blotting and quantified by densitometry. A representative immunoblot from four independent experiments is shown (left panel) and the quantification of these proteins are shown on the right. All values are presented as mean±S.D. of four independent experiments. ** $p<0.01$, *** $p<0.001$ *vs.* control.

ABCA1 expression. In addition, there are two possibilities that honokiol-bound-RXRβ-mediated increase in ABCA1 expression. One is that honokiol-bound RXRβ activates PPARs/RXR heterodimer, which subsequently activates LXRα, and another one is that it directly activates LXR/RXR heterodimer to increase ABCA1 expression.

Honokiol Increases the Expression Levels of ABCA1, ABCG1 and Apolipoprotein E in THP-1 Macrophages Next, we also examined the effect of honokiol on ABCA1 expression in other cell types including THP-1 macrophages, rat primary neurons and astrocytes. ABCA1 mRNA and protein levels were increased by 3- and 3-fold in THP-1 macrophages (Fig. 5). It has also been reported that the expressions of ABCG1, another ATP-binding cassette transporter, and apoE are mediated *via* the LXR/RXR pathway in THP-1 macrophages.[24] We determined whether honokiol can also increase the ABCG1 and apolipoprotein E (apoE) expression levels in THP-1 macrophages because honokiol activates RXRβ as observed earlier. Honokiol increased the ABCG1 and apoE mRNA levels by 2.9- and 3-fold, respectively (Fig. 5A), and their protein levels were increased by 4.5- and 7-fold, respectively (Fig. 5B). In addition to THP-1 macrophage, we observed that honokiol treatment enhanced ABCA1 mRNA and protein levels by 5- and 6-fold in rat primary neurons (Figs. 6A, B), and by 2- and 2.2-fold, respectively, in rat primary astrocytes (Figs. 6C, D), although an honokiol-induced ABCA1 expression levels in primary astrocytes were relatively low compared with those in primary neurons. Since astrocytes are major source of apoE in the brain, we determined whether honokiol can increase the apoE expression levels in primary astrocytes. Honokiol treatment increased the apoE protein levels by 2.3-fold in these cells (Fig. 6D). To determine whether honokiol treatment enhances brain HDL generation and attenuates Aβ burden in APP-transgenic mice also remains to be addressed.

Acknowledgements This work was supported by Grants from the Ministry of Health, Labor and Welfare of Japan (Comprehensive Research on Aging and Health (H20-007), and the Program for Promotion of Fundamental Studies in

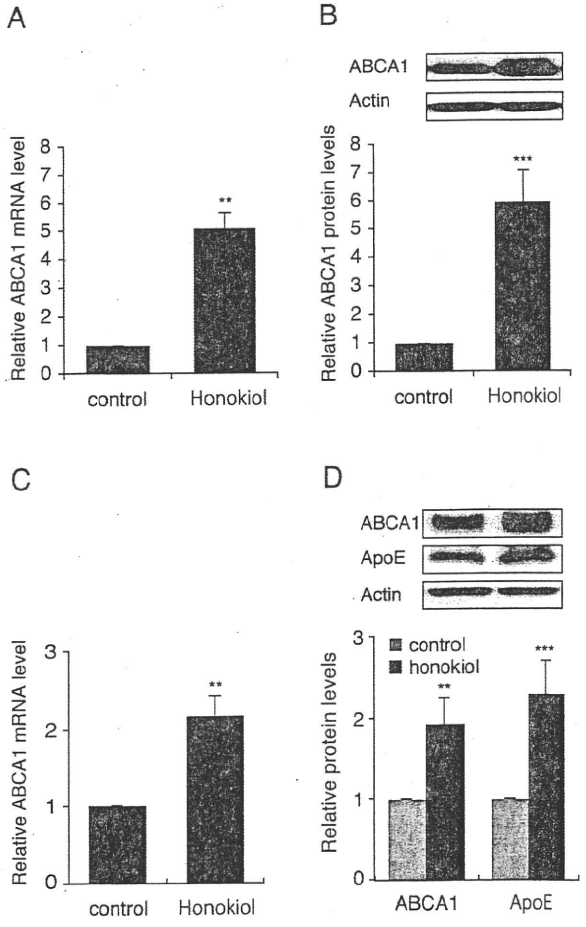

Fig. 6. Honokiol Increased the Expression Levels of ABCA1 and apoE in Primary Rat Neurons and Astrocytes

Primary rat neurons (A, B) and astrocytes (C, D) were treated with 10 mM honokiol or vehicle control (0.1% DMSO) for 24 h. The cells were harvested and used for the determination of ABCA1 mRNA level by real-time PCR analysis (A, C). ABCA1 protein levels in neurons (B) and astrocytes (D), and apoE protein levels in astrocytes (D) were determined by Western blot analysis. A representative immunoblot from three independent experiments is shown (upper panel) and the quantification of ABCA1 protein is shown on the lower graph (B, D). Real-time PCR and Western blot analysis were performed as described in the legend for Fig. 5. All values are presented as mean±S.D. of three independent experiments. ** $p<0.01$, *** $p<0.001$ *vs.* control.

Health of the National Institute of Biomedical Innovation (NIBIO), A Grant-in-Aid for Scientific Research on Priority Areas—Research on Pathomechanisms of Brain Disorders—from the Ministry of Education, Culture, Sports, Science and Technology of Japan (20023040).

REFERENCES

1) Oram J. F., Lawn R. M., *J. Lipid Res.*, **42**, 1173—1179 (2001).
2) Brooks-Wilson A., Marcil M., Clee S. M., Zhang L. H., Roomp K., van Dam M., Yu L., Brewer C., Collins J. A., Molhuizen H. O., Loubser O., Ouelette B. F., Fichter K., Ashbourne-Excoffon K. J., Sensen C. W., Scherer S., Mott S., Denis M., Martindale D., Frohlich J., Morgan K., Koop B., Pimstone S., Kastelein J. J., Genest J. Jr., Hayden M. R., *Nat. Genet.*, **22**, 336—345 (1999).
3) Mott S., Yu L., Marcil M., Boucher B., Rondeau C., Genest J. Jr., *Atherosclerosis*, **152**, 457—468 (2000).
4) Krimbou L., Denis M., Haidar B., Carrier M., Marcil M., Genest J. Jr., *J. Lipid Res.*, **45**, 839—848 (2004).
5) Borghini I., Barja F., Pometta D., James R. W., *Biochim. Biophys. Acta*, **1255**, 192—200 (1995).
6) Wahrle S. E., Jiang H., Parsadanian M., Legleiter J., Han X., Fryer J. D., Kowalewski T., Holtzman D. M., *J. Biol. Chem.*, **279**, 40987—40993 (2004).
7) Wahrle S. E., Jiang H., Parsadanian M., Hartman R. E., Bales K. R., Paul S. M., Holtzman D. M., *J. Biol. Chem.*, **280**, 43236—43242 (2005).
8) Wahrle S. E., Jiang H., Parsadanian M., Kim J., Li A., Knoten A., Jain S., Hirsch-Reinshagen V., Wellington C. L., Bales K. R., Paul S. M., Holtzman D. M., *J. Clin. Invest.*, **118**, 671—682 (2008).
9) Murthy S., Born E., Mathur S. N., Field F. J., *J. Lipid Res.*, **43**, 1054—1064 (2002).
10) Chawla A., Boisvert W. A., Lee C. H., Laffitte B. A., Barak Y., Joseph S. B., Liao D., Nagy L., Edwards P. A., Curtiss L. K., Evans R. M., Tontonoz P., *Mol. Cell*, **7**, 161—171 (2001).
11) Schmitz G., Langmann T., *Biochim. Biophys. Acta*, **1735**, 1—19 (2005).
12) Costet P., Luo Y., Wang N., Tall A. R., *J. Biol. Chem.*, **275**, 28240—28245 (2000).
13) Joseph S. B., McKilligin E., Pei L., Watson M. A., Collins A. R., Laffitte B. A., Chen M., Noh G., Goodman J., Hagger G. N., Tran J., Tippin T. K., Wang X., Lusis A. J., Hsueh W. A., Law R. E., Collins J. L., Willson T. M., Tontonoz P., *Proc. Natl. Acad. Sci. U.S.A.*, **99**, 7604—7609 (2002).
14) Jiang Q., Lee C. Y., Mandrekar S., Wilkinson B., Cramer P., Zelcer N., Mann K., Lamb B., Willson T. M., Collins J. L., Richardson J. C., Smith J. D., Comery T. A., Riddell D., Holtzman D. M., Tontonoz P., Landreth G. E., *Neuron*, **58**, 681—693 (2008).
15) Michikawa M., Gong J. S., Fan Q. W., Sawamura N., Yanagisawa K., *J. Neurosci.*, **21**, 7226—7235 (2001).
16) Zhang J. H., Chung T. D., Oldenburg K. R., *J. Biomol. Screen*, **4**, 67—73 (1999).
17) Koldamova R. P., Lefterov I. M., Ikonomovic M. D., Skoko J., Lefterov P. I., Isanski B. A., DeKosky S. T., Lazo J. S., *J. Biol. Chem.*, **278**, 13244—13256 (2003).
18) Bai X., Cerimele F., Ushio-Fukai M., Waqas M., Campbell P. M., Govindarajan B., Der C. J., Battle T., Frank D. A., Ye K., Murad E., Dubiel W., Soff G., Arbiser J. L., *J. Biol. Chem.*, **278**, 35501—35507 (2003).
19) Yang S. E., Hsieh M. T., Tsai T. H., Hsu S. L., *Biochem. Pharmacol.*, **63**, 1641—1651 (2002).
20) Fukuyama Y., Nakade K., Minoshima Y., Yokoyama R., Zhai H., Mitsumoto Y., *Bioorg. Med. Chem. Lett.*, **12**, 1163—1166 (2002).
21) Quinn C. M., Kagedal K., Terman A., Stroikin U., Brunk U. T., Jessup W., Garner B., *Biochem. J.*, **378**, 753—761 (2004).
22) Hahm E. R., Singh S. V., *Mol. Cancer Ther.*, **6**, 2686—2695 (2007).
23) Mascrez B., Ghyselinck N. B., Watanabe M., Annicotte J. S., Chambon P., Auwerx J., Mark M., *EMBO Rep.*, **5**, 285—290 (2004).
24) Beyea M. M., Heslop C. L., Sawyez C. G., Edwards J. Y., Markle J. G., Hegele R. A., Huff M. W., *J. Biol. Chem.*, **282**, 5207—5216 (2007).

BRAIN RESEARCH 1355 (2010) 165–173

available at www.sciencedirect.com

ScienceDirect

www.elsevier.com/locate/brainres

BRAIN RESEARCH

Research Report

Treadmill running improves motor function and alters dendritic morphology in the striatum after collagenase-induced intracerebral hemorrhage in rats

Yasuyuki Takamatsu[a], Akimasa Ishida[a], Michiru Hamakawa[a], Keigo Tamakoshi[a], Cha-Gyun Jung[b], Kazuto Ishida[a,*]

[a]Department of Physical Therapy, Program in Physical and Occupational Therapy, Nagoya University Graduate School of Medicine, Nagoya, Aichi, Japan

[b]Department of Alzheimer's Disease Research, National Institute for Longevity Sciences, National Center for Geriatrics and Gerontology, Obu, Aichi, Japan

ARTICLE INFO

Article history:
Accepted 19 July 2010
Available online 24 July 2010

Keywords:
Intracerebral hemorrhage
Striatum
Treadmill running
Dendrite
PSD-95

ABSTRACT

It is well known that early rehabilitation is effective for functional recovery after intracerebral hemorrhage (ICH); however, the mechanisms have not been well described. The purpose of this study was to elucidate the effects of early rehabilitative therapy (treadmill running) on recovery of motor function and alteration of brain histology after ICH. Male Wistar rats, under deep anesthesia, were placed in a stereotaxic apparatus and injected with collagenase into the left striatum to induce ICH. Sham operated animals were treated with saline. All animals were randomly assigned to treadmill exercise (for 30 min/day, 9 m/min, between 4 and 14 days after surgery) and control and were designated to one of four groups: sham+control (SC), sham+treadmill (ST), ICH+control (IC), ICH+treadmill (IT). Motor deficit score (MDS) was assessed daily after surgery. Volume of tissue lost, dendritic morphology and PSD-95 protein level in the striatum were analyzed at 15 days after surgery. The MDS of IT was significantly improved compared with IC over time. There were no differences between IT and IC in the volume of tissue lost (IT: 63.8%, IC: 61.8%), spine density or PSD-95 protein level in the striatum. However, dendritic length was increased and arborization was more complex in the contralateral striatum of the IT than the IC group (IT: 1226 μm, IC: 937 μm). These data suggest that treadmill running improves motor function after ICH and that improvement may be related to alteration of dendritic morphology in the striatum.

1. Introduction

Intracerebral hemorrhage (ICH) is a cerebral vascular accident characterized by long-term impairments of motor function and activities of daily living (ADL) that affects approximately 10–15% of all patients with strokes (Sudlow et al., 1997). As of recently, it is strongly recommended that rehabilitative therapy (physical and occupational therapy) is started as

* *Corresponding author.* 1-1-20 Daikominami, Higashi-ku, Nagoya 461-8673, Japan. Fax: +81 52 719 1343.
E-mail address: ishida@met.nagoya-u.ac.jp (K. Ishida).

Abbreviations: ICH, intracerebral hemorrhage; MDS, motor deficit score; PSD-95, postsynaptic density 95; SC, sham+control; ST, sham+treadmill; IC, ICH+control; IT, ICH+treadmill

0006-8993/$ – see front matter © 2010 Elsevier B.V. All rights reserved.
doi:10.1016/j.brainres.2010.07.070

early as possible to improve their motor function and ADL (Johansson, 2000; Thorsén et al., 2005; Langhorne et al., 2005; Langhorne et al., 2007). Thus, early intervention for mobilization and training following stroke are well accepted clinically. A previous study indicated that early exclusive use of an affected limb exacerbates brain damage after focal brain ischemia (Risedal et al., 1999). However, many reports show the benefit of exercise at early stage. Early treadmill running after middle cerebral artery occlusion improved motor function and reduced infarct volume (Yang et al., 2003). Similarly, in an ICH model, early treadmill running induced recovery of motor function and reduction of lesion volume (Lee et al., 2003; 2005; Park et al., 2010). So, early treadmill running may have not only benefited motor function but also provided neuroprotection after ICH. However, the mechanisms of improved motor function by treadmill running after ICH are incompletely understood.

It is reported that neuronal plasticity contributes to the recovery of motor function after brain injury resulting from stoke or head trauma. Animal studies showed that the cellular and molecular events underlying spontaneous recovery after brain injury include structural changes in axons, dendrites, or synapses. Nguyen et al. (2008) reported that dendritic length and arborization increased in the contralateral striatum after ICH in rats. Furthermore, previous studies have shown that rehabilitation (enriched environment, reaching training of affected limb) improved motor function and enhanced changes in dendritic structure and complexity in the contralateral hemisphere after brain injury (Biernaskie et al., 2001; Jones et al., 1994; Bury et al., 2000). So, alterations of dendritic morphology in the contralateral hemisphere have been implicated in recovery of motor function after brain injury. Additionally, changes in synaptic activity as indicated by long-term potentiation (LTP) have been reported to contribute to brain reorganization after stroke. PSD-95, a synaptic scaffolding protein with multiple protein–protein interaction domains, is enriched in the postsynaptic density (PSD) and is an important regulator of synaptic strength and plasticity (Sheng et al., 2002; Han et al., 2008; Sheng et al., 2007). Previous studies have shown that running exercise induced changes in dendritic structure (Redila et al., 2006; Stranahan et al., 2007) and increased PSD-95 protein level (Dietrich et al., 2005; Hu et al., 2009) in normal rats. Therefore, running exercise is assumed to evoke brain plasticity. However, the effect of running exercise on dendritic morphology and PSD-95 protein level after ICH in rats has not been described.

The purpose of the present study was to investigate the effect of treadmill running on motor function and plastic changes in the striatum, focusing on dendritic morphology and PSD-95 protein level, after collagenase induced ICH in rats.

2. Results

2.1. *Motor deficit score (MDS)*

Animals had motor deficit after ICH that recovered over time. Furthermore, MDS of ICH+treadmill (IT) animals significantly improved compared with ICH+control (IC) animals by 15 days after ICH. Notably, there were significant differences between IT and IC animals at 7–15 days after ICH (7, 9–10 days, $p<0.05$; 8, 11–15 days, $p<0.01$. Fig. 1). MDS of each group were the same extent among experiments, such as H–E staining, Golgi-Cox staining and PSD-95 analysis.

2.2. *Striatal volume loss*

Striatal volume loss in ICH animals (IC, IT) was more than that of sham animals (sham+control, SC: sham+treadmill, ST) at 15 days after surgery ($p<0.05$). However, there were no significant differences between IT and IC animals (Fig. 2).

2.3. *Alteration of dendritic morphology*

In the ipsilateral striatum (Fig. 4A), IC animals had fewer intersections 140 μm from the cell body compared with ST animals ($p<0.05$). IT animals had fewer intersections 120 and 140 μm from the cell body as compared with ST animals ($p<0.05$). However, there were no significant differences between IT and IC animals. In the contralateral striatum (Fig. 4B), IC animals had a greater number of intersections 60 μm from the cell body compared with ST animals. IT animals had a greater number of intersections at 40, 60, and 80 μm from the cell body as compared with SC and ST animals ($p<0.05$). Furthermore, at 20 and 40 μm from the cell body, IT animals had a greater number of intersections compared with IC animals ($p<0.05$), (Fig. 3).

Total dendritic length in the ipsilateral striatum was not significantly different between groups (Fig. 5A). However, in the contralateral striatum, total dendritic length of IT animals was significantly longer than that of SC, ST and IC animals ($p<0.05$, Fig. 5B).

Spine density (number of spines/μm dendrite) was significantly lower in IC than SC and ST animals in the ipsilateral striatum ($p<0.05$), but there were no significant differences

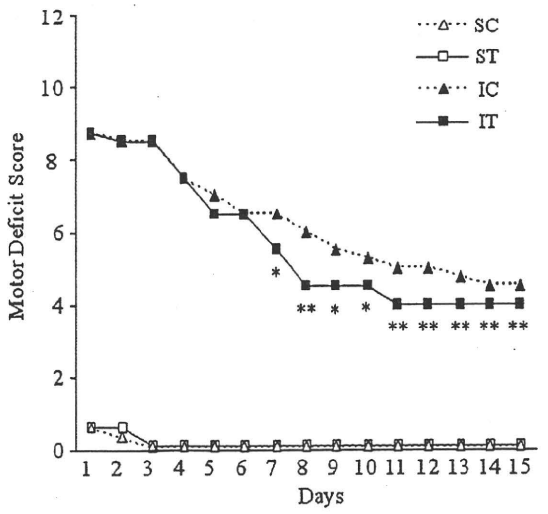

Fig. 1 – Change in motor deficit score (MDS) after ICH. Median values are shown. MDS of IT animals significantly improved compared with IC, especially between 7 and 15 days after ICH. *$p<0.05$, **$p<0.01$ compared with IC at each time point with Mann–Whitney U. SC: sham control group, ST: sham treadmill group, IC: ICH control group, IT: ICH treadmill group.

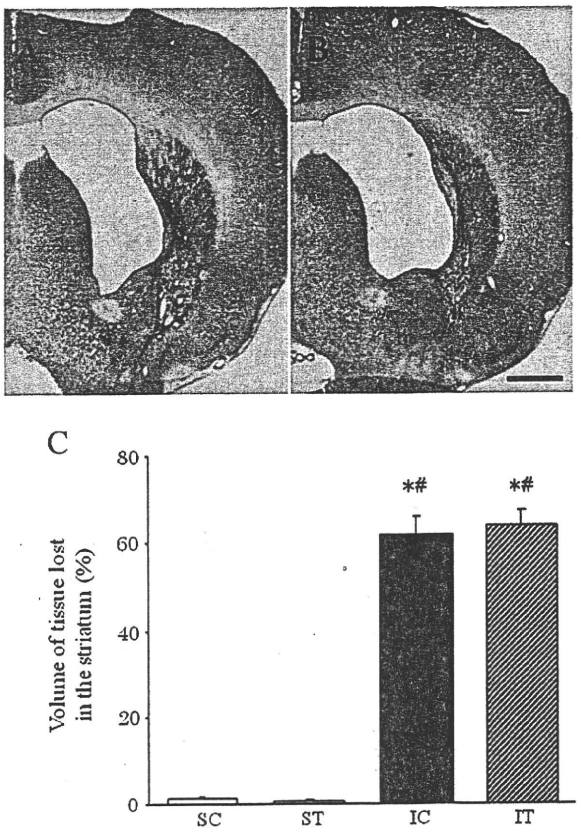

Fig. 2 – Photomicrographs showing H–E staining in the striatum. (A) ICH control group; (B) ICH treadmill group. Scale bar, 2 mm. (C) Volume of tissue lost in the striatum (%) at 15 days after ICH. Values are represented as the mean ± SEM. There was no difference between IC and IT. *$p<0.01$ compared with SC. #$p<0.01$ compared with ST. SC: sham control group, ST: sham treadmill group, IC: ICH control group, IT: ICH treadmill group.

between IT, SC, and ST animals (Fig. 6A). In the contralateral striatum, the spine density of IC and IT animals was more than that of SC and ST animals ($p<0.05$), but there were no there were no significantly differences between IT and IC animals (Fig. 6B).

2.4. *Expression profile of PSD-95*

PSD-95 protein level expressed as ratio of SC animals and was normalized for β-actin protein level. ST animals had the highest protein levels in both ipsilateral and contralateral striatum, but no significant differences existed between groups (Fig. 7).

3. Discussion

Recovery of motor function is promoted by rehabilitative exercise, such as treadmill running, following stroke. The present study examined the effect of treadmill running (from 4 to 14 days after ICH) on motor function and brain histology after ICH in rats. We demonstrated that treadmill running improved MDS after ICH (Fig. 1). In addition to recovery of motor function, we showed that treadmill running induced alterations in dendritic morphology (dendritic arborization and length) in the contralateral striatum for the first time that we are aware of. However, the volume of striatal tissue loss was unchanged. Moreover, spine density and PSD-95 protein levels were the same between treadmill and control groups after ICH. These findings suggest that treadmill running improves motor function after ICH and that this improvement may be related to alteration of dendritic morphology in the contralateral striatum.

Early treadmill training could be neuroprotective following ICH. The results of a previous study indicated that treadmill exercise from 1 to 11 days after collagenase injection decreased lesion volume and the number of caspase-3 positive cells in the striatum (Lee et al., 2003). Furthermore, early treadmill, which started 24 h after ICH, was more effective at recovering motor function and reducing lesion volume than late treadmill, which started 3 days to 1 week after ICH. (Lee et al., 2005; Park et al., 2010). However, we found no effect of treadmill running from 4 to 14 days after ICH on striatal volume loss (Fig. 2). This training may not have been effective at reducing tissue loss because treadmill running started relatively late, 4 days, after ICH. On the other hand, motor function, such as MDS, was improved by treadmill running. Thus, treadmill running may have benefited recovery of motor function even though tissue loss in the striatum was not prevented after ICH.

To our knowledge, this study is the first investigation to demonstrate an effect of treadmill running on dendritic morphology in the striatum after ICH. One previous study examined dendritic morphology over the course of spontaneous recovery after ICH, and reported that there was an enhancement in dendritic arborization in the contralateral striatum at seven and 60 days following ICH without rehabilitative training (Nguyen et al., 2008). Similarly, our data showed that dendritic arborization in the contralateral striatum of ICH animals was more complex than that of sham animals 15 days following ICH (Figs. 3, 4 and 5). Furthermore, we showed that spine density was higher in ICH animals than sham animals (Fig. 6). Increased dendritic complexity and spine density have been associated with recovery after brain injury (Johansson, 2000; Kleim et al., 2003), and plastic (dendritic) changes in the contralateral hemisphere have been implicated in functional recovery (Calautti and Baron, 2003; Noskin et al., 2008; Teasell et al., 2006). Unilateral intra-cerebral hemorrhage-induced degenerative events might have promoted neuronal activity and upregulated the expression of neurotrophic factors in the contralateral hemisphere. Reorganization of new neuronal circuits may have occurred to compensate for functional disturbances, resulting in enhancement of dendritic complexly and spine density in the striatum contralateral to the lesion. Furthermore, an increase in dendritic complexly or spine density in the contralateral striatum might have an important role in spontaneous recovery of motor function after ICH. In this study, treadmill running enhanced the increase in dendritic arborization and length in the contralateral striatum after ICH (Figs. 3, 4 and 5). After brain injury, dendritic complexly and length was increased in the contralateral hemisphere, which was further enhanced by rehabilitative training (Biernaskie et al., 2001; Jones et al., 1994; Bury et al., 2000). Some reports have shown that running exercise or enriched environments increase

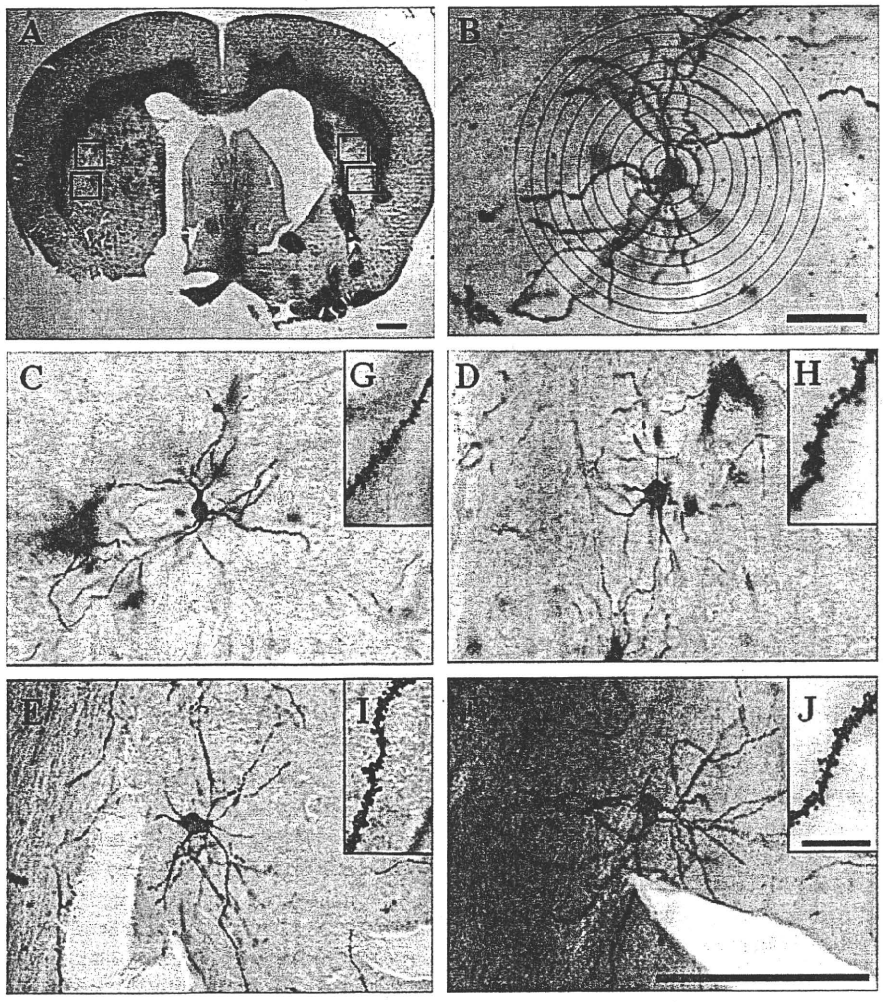

Fig. 3 – Photomicrographs showing Golgi-Cox staining. (A) Region of analyzed neurons in the ipsilateral and contralateral striatum. (B) Sholl analysis. Medium-sized spiny neurons and spines of (C, G) sham control group, (D, H) sham treadmill group, (E, I) ICH control group and (F, J) ICH treadmill group in the contralateral striatum. Scale bars: A, 1 mm; B, 200 μm; 200 μm for C–F in F; 10 μm for G–J in J.

neurotrophic factors (Ang et al., 2003). Levels of neurotrophins such as brain-derived neurotrophic factor (BDNF) (Soya et al., 2007; Kim et al., 2005; Molteni et al., 2002) and vascular endothelial growth factor (VEGF) (Lou et al., 2008) are increased in exercised animals compared with controls. Increased neurotrophin levels have been postulated to promote synaptic neuroplasticity (McAllister et al., 1999). Thus, treadmill running may prove to increase production of neurotrophic factors that can alter dendritic processing in the striatum. Furthermore, dendritic growth in the hemisphere opposite the lesion peaks 2–3 weeks after brain injury (Jones et al., 1992). Therefore, treadmill running started 4–14 days after ICH, before the peak in dendritic growth, may be effective at increasing dendritic arborization and length.

It has been previously reported that running exercise increases extracellular glutamate levels (Chang et al., 2009), phosphorylation of N-methyl-D-aspartic acid receptors (NMDAR) (Dietrich et al., 2005), BDNF expression (Soya et al., 2007; Kim et al., 2005; Molteni et al., 2002) and PSD-95 protein (Hu et al., 2009; Dietrich et al., 2005) within the brain. PSD-95 is transported to dendrites following activating the NMDAR-BDNF-PI3K pathway (Yoshii et al., 2007). Therefore, we hypothesized that treadmill running would induce PSD-95 expression by activating the NMDAR-BDNF-PI3K pathway. However, we did not find that significant differences in the PSD-95 level in the striatum were induced by treadmill running after ICH (Fig. 7). A previous study showed that plastic changes in the synapse began 2–3 weeks after brain injury and peaked 1 month after (Jones et al., 1996). Enforcement of treadmill running, from 4 to 14 days after ICH, might be too early or short to change PSD-95 protein levels because synaptic changes might not have occurred by 15 days after ICH. Treadmill running might require a longer intervention period to activate PSD-95 expression following ICH.

Our study has several limitations. First, we examined only one behavior test, MDS, in this study. MDS is a useful but gross measure for assessing neurological deficit but may not be the most sensitive neurological scale for use after brain injury. Further studies should examine motor functional recovery in greater detail by other behavioral tests, such as

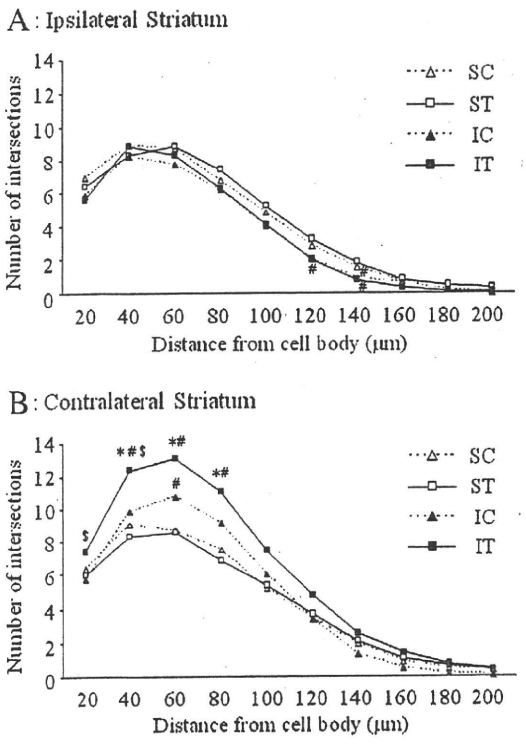

Fig. 4 – Dendritic arborization measured by Sholl analysis both ipsilateral (A) and contralateral (B) to injured striatum 15 days after ICH. In the ipsilateral striatum, there was little difference between any groups (A). In the contralateral striatum, dendritic arborization in ICH groups (IC, IT) was more complex than sham groups (SC, ST). Furthermore, the dendritic arborization of IT significantly increased compared with that of IC (B). Values are represented as the mean ± SEM. *$p<0.05$ compared with SC. #$p<0.05$ compared with ST. $$p<0.05$ compared with IC. SC: sham control group, ST: sham treadmill group, IC: ICH control group, IT: ICH treadmill group.

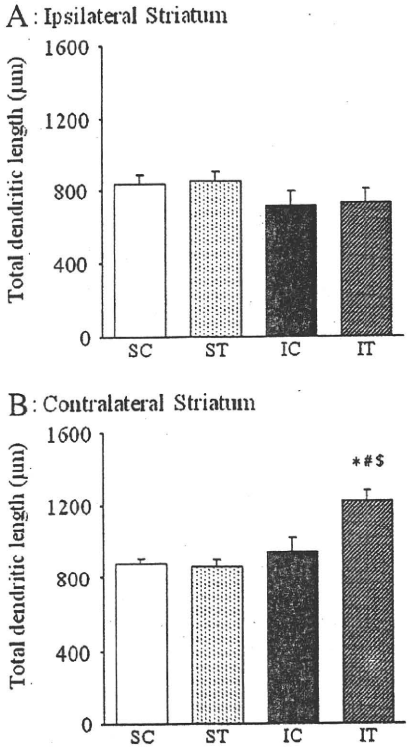

Fig. 5 – Total dendritic length measured by Sholl analysis both ipsilateral (A) and contralateral (B) to injured striatum 15 days after ICH. In the ipsilateral striatum, there were no differences between any groups (A). In the contralateral striatum, the total dendritic length of IT increased significantly compared with that of other groups (B). Values are represented as the mean ± SEM. *$p<0.05$ compared with SC. #$p<0.05$ compared with ST. $$p<0.05$ compared with IC. SC: sham control group, ST: sham treadmill group, IC: ICH control group, IT: ICH treadmill group.

the single pellet reaching test (Whishaw et al., 1990), staircase skilled-reaching test (Montoya et al., 1991), and horizontal ladder rung walking test (Metz and Whishaw, 2002). Second, we examined only relatively short-term (2 weeks) benefits of treadmill running after ICH and showed transient effects on motor functional recovery and alternation of dendritic morphology. It is unclear whether the effects of treadmill running on motor functional recovery and alternation of dendritic morphology is transient or permanent. We have reported some MDS data on animals followed up long-term after ICH (Kato et al., 2004). In our previous data, we found that the improvement remained 4 but not 6 weeks after ICH. We believe that further studies are necessary to assess longer-term follow-up data in detail. Third, we did not show the mechanisms by which dendritic morphology are altered after ICH and enhanced by treadmill running. Future studies should consider additional experiments examining the role of neurotrophins (BDNF, NGF, VEGF), which contribute to neuronal plasticity. In our study, it was unclear whether treadmill running induced neurotrophins sufficiently to alter dendritic morphology. For example, the intensity of running seems to be an important factor in neurotrophin expression. It was reported that low intensity running increased BDNF in the rat hippocampus more than moderate intensity (Soya et al., 2007). Additional data about neurotrophins or other molecules involved in neuronal plasticity is needed to determine why dendritic arborization was enhanced by treadmill running. Further studies are needed to determine the extent to which treadmill running increases neurotrophins, and the optimum intensity of treadmill running for effective recovery of motor function and neuronal plasticity after ICH. We need to find the "optimum conditions" for exercise for recovery of motor function and neuronal plasticity, and consider implementing them in patients with ICH who have motor impairment and require rehabilitation.

In summary, we demonstrated that treadmill running after ICH in rats improved motor function and enhanced the alteration of dendritic morphology (dendritic arborization and length) in the contralateral striatum. However, treadmill running after ICH did not change volume of tissue lost, spine density, or PSD-95 protein level in the striatum. These data

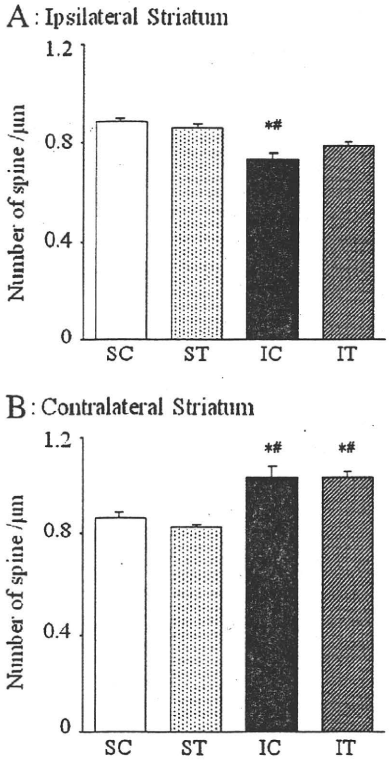

Fig. 6 – Spine density ipsilateral (A) and contralateral (B) to injured striatum 15 days after ICH. In the ipsilateral striatum, the spine density of IC was significantly lower than that of sham groups (SC, ST), but there were no differences between IT and sham groups (A). In the contralateral striatum, the spine density of ICH groups (IC, IT) was more than that of sham groups (SC, ST), but there was no difference between IC and IT (B). Values are represented as the mean±SEM. $^{*}p<0.05$ compared with SC. $^{\#}p<0.05$ compared with ST. $^{\$}p<0.05$ compared with IC. SC: sham control group, ST: sham treadmill group, IC: ICH control group, IT: ICH treadmill group.

suggest that the improvement in motor function after treadmill running might result in alterations of dendritic morphology in the contralateral striatum after ICH.

4. Experimental procedures

4.1. *Animals models*

Male Wistar rats weighing 240–270 g (8 weeks of age) were used. Rats were housed at 25 °C during a 12 h light/dark cycle, with food and water made available ad libitum throughout the experiments. Animal care and surgical procedures were performed in accordance with the animal care guidelines of the Nagoya University. All efforts were made to minimize suffering and the number of animals used. They were randomly assigned to sham or ICH. Each group was divided into two subgroups: treadmill exercise and control (no exercise) groups. Therefore, four groups were included in this study: SC, ST, IC, and IT. Animals within each group were randomly assigned to three analysis groups: Hematoxylin–Eosin (H–E) staining, Golgi-Cox staining and Western blotting.

4.2. *Induction of ICH*

We used the bacterial collagenase model of ICH based on previous studies with minor modifications (Rosenberg et al., 1990; Del Bigio et al., 1996). To induce hemorrhage, rats were anesthetized with sodium pentobarbital (45 mg/kg, i.p.) and placed on a stereotaxic frame. Through a hole drilled in the skull, a needle (φ=400 μm) was implanted into the striatum at the following coordinates: 3.0 mm lateral to the midline, 0.2 mm anterior to the coronal suture, and depth 6.0 mm deep from the surface of the brain. 1.2 μl saline containing 0.24 U of collagenase (Type IV; Sigma-Aldrich, St. Louis, MO, USA) was infused over 6 min. The needle remained in place for an additional 7 min after the infusion and was subsequently withdrawn slowly. Sham operated animals were injected with 1.2 μl of saline instead of collagenase.

4.3. *Behavioral testing*

Motor behavior was evaluated using four tests in each rat from days 1 to 15 after ICH induction. The specific tests included (1) observation of spontaneous ipsilateral circling, graded from 0 (no circling) to 3 (continuous circling); (2) contralateral hindlimb retraction, which measured the ability of the animal to replace the hindlimb after it was displaced laterally by 2–3 cm, graded from 0 (immediate replacement) to 3 (replacement after minutes or no replacement); (3) beam walking ability, graded 0 for a rat that readily traverses a 2.4-cm-wide, 80-cm-long beam to 3 for a rat unable to stay on the beam for 10 s; and (4) bilateral forepaw grasp, which measures the ability to hold onto a 2-mm diameter steel rod, graded 0 for a rat with normal forepaw grasping behavior to 3 for a rat unable to grasp with the forepaws. The scores from all four tests were added to give a motor deficit score (MDS; maximum possible score, 12) (Altumbabic et al., 1998).

4.4. *Treadmill exercise*

Animals in the treadmill groups (ST and IT) were forced to run on a motorized treadmill for 30 min at a speed of 9 m/min once a day. The treadmill groups were scheduled to run on a treadmill from days 4 to 14 after ICH induction, 11 consecutive days. Animals in the control groups (SC and IC) were left in the treadmill without running for the same period as the treadmill groups. All animals were forced to run after behavioral tests had finished.

4.5. *H–E staining*

At 15 days after surgery, animals (SC, n=8; ST, n=8; IC, n=6; IT, n=7) were randomly selected, placed under deep anesthesia with sodium pentobarbital (45 mg/kg, i.p.), transcardially perfused with 0.9% saline, and subsequently